

Critical and Tricritical Hard Objects on Bicolorable Random Lattices: Exact Solutions

J. Bouttier¹, P. Di Francesco² and E. Guitter³

*CEA-Saclay, Service de Physique Théorique,
F-91191 Gif sur Yvette Cedex, France*

We address the general problem of hard objects on random lattices, and emphasize the crucial role played by the colorability of the lattices to ensure the existence of a crystallization transition. We first solve explicitly the naive (colorless) random-lattice version of the hard-square model and find that the only matter critical point is the non-unitary Lee-Yang edge singularity. We then show how to restore the crystallization transition of the hard-square model by considering the same model on bicolored random lattices. Solving this model exactly, we show moreover that the crystallization transition point lies in the universality class of the Ising model coupled to 2D quantum gravity. We finally extend our analysis to a new two-particle exclusion model, whose regular lattice version involves hard squares of two different sizes. The exact solution of this model on bicolorable random lattices displays a phase diagram with two (continuous and discontinuous) crystallization transition lines meeting at a higher order critical point, in the universality class of the tricritical Ising model coupled to 2D quantum gravity.

01/02

¹ bouttier@spht.saclay.cea.fr

² philippe@spht.saclay.cea.fr

³ gutter@spht.saclay.cea.fr

1. Introduction

In lattice statistical mechanics, universality classes usually do not depend on the lattice over which the model is defined, but only on the symmetries of the interactions. The situation however becomes more subtle when the symmetries of the interactions themselves strongly depend on the properties of the underlying lattice. A famous example of such behavior is provided by the general problem of “hard” objects on two-dimensional lattices. In these models, each site of the lattice may be in two states, occupied or empty, but if a site is occupied, then necessarily its nearest neighbors must be empty. The models are further defined by attaching an activity z per occupied vertex. For regular lattices in two dimensions, an exact solution for the thermodynamics of the model exists so far only in the case of the triangular lattice (hard hexagon model, solved by Baxter [1]). In this case, two critical points were found at values $z_{\pm} = \left(\frac{1 \pm \sqrt{5}}{2}\right)^5$, $z_- < 0$, $z_+ > 0$, respectively governed by the Lee-Yang edge singularity in 2D [2,3] (non-unitary Conformal Field Theory (CFT) with central charge $c(2,5) = -22/5$) and the critical three-state Potts model (unitary CFT with central charge $c(5,6) = 4/5$). Despite recent progress [4,5], the hexagonal lattice and square lattice cases remain elusive [6]. Numerical evidence however seems to indicate that they still have two critical points $z_- < 0$ and $z_+ > 0$, and while the first still corresponds to the Lee-Yang edge singularity, the other one displays the exponents of the critical Ising model [4] (CFT with $c(3,4) = 1/2$). The difference in universality class at z_+ for the triangular lattice on one hand and the hexagonal or square lattice on the other may be simply understood from the symmetries of the lattices. Indeed, this critical point corresponds in all cases to a crystallization transition, where the hard particles occupy preferentially a particular sublattice of the lattice at hand. The common feature of the square and hexagonal lattice is their vertex-bicolorability (bipartite nature) which naturally defines two equivalent mutually excluding sublattices corresponding to two possible symmetric crystalline groundstates. The triangular lattice on the other hand is not vertex-bicolorable, but vertex-tricolorable instead, which allows to define three equivalent mutually excluding sublattices corresponding to three possible symmetric crystalline states. These two- or three-fold symmetries give rise naturally to critical points with \mathbb{Z}_2 (Ising) or \mathbb{Z}_3 (three-state Potts) symmetries.

The purpose of this note is to study similar hard particle models on random lattices such as those used to generate discrete models of 2D quantum gravity. The aim of this study is twofold: (1) to check the crucial role played by the vertex-colorability of the

underlying lattices in determining the physical behavior of the models and (2) to give a “gravitational” proof that the crystallization transition point z_+ indeed lies in the critical Ising universality class in the case of hard particles on bicolorable lattices.

More precisely, in this paper, we first solve explicitly the problem of hard particles on arbitrary random lattices and show that in the absence of any colorability constraint (Euclidean random surfaces), only the Lee-Yang critical point survives at some negative value $z = z_-$. We then solve the same model on so-called Eulerian random surfaces, i.e. random lattices for which we impose vertex-bicolorability, and find that the crystallization transition point $z = z_+$ is restored in this case, and that it belongs to the universality class of the critical Ising model coupled to 2D quantum gravity.

We next extend our analysis to higher order critical points and show how to recover the tricritical Ising universality class (CFT with central charge $c(4, 5) = 7/10$) by considering a *two-particle* exclusion model on vertex-bicolorable lattices. We again give a gravitational proof of this fact by explicitly solving the model on random vertex-bicolorable lattices.

The paper is organized as follows. In Sect. 2 we study the model of hard particles and first recall a few known facts on its regular honeycomb and square lattice version (Sect. 2.1). We then solve the model in Sect. 2.2 on arbitrary random planar tetravalent lattices, by use of a two-matrix integral. In addition to the activity z per particle, the latter include an extra weight g per vertex (occupied or not). We derive explicitly the gravitational critical line $g = g_c(z)$ selecting arbitrarily large lattices, allowing to reach the interesting thermodynamic behavior of the model. On this line, we find a unique critical point of the matter system at some $z = z_-$, which we identify as the Lee-Yang edge singularity. In Sect. 2.3, we introduce a four-matrix model describing the same problem now on random vertex-bicolorable lattices. We solve this model exactly in the case of trivalent such lattices and obtain in particular the new gravitational critical line $g = g_c(z)$. Along this line, we now find two matter critical points at some values $z = z_- < 0$ and $z = z_+ > 0$. The first one is still identified as the Lee-Yang edge singularity, while the new one is identified as a crystallization transition point in the universality class of the critical Ising model. Sect. 3 is devoted to the study of a more sophisticated two-particle exclusion model in which we allow sites to be occupied by single particles (with activity z_1 per particle) or pairs of particles (with activity z_2 per pair), while the exclusion rule imposes that each edge of the lattice is shared by a total of *at most* two particles. In Sect. 3.1, we present its expected phase diagram on a regular square or honeycomb lattice obtained by applying the same ideas as above, i.e. relating the different phases of the model to the compatibility

between the exclusion rules on one hand and the vertex-bicolorability of the lattice on the other. These ideas are tested in Sect. 3.2 where we solve the model on random trivalent vertex-bicolorable lattices, by means of a six-matrix integral. The gravitational critical surface $g = g_c(z_1, z_2)$ is explicitly shown to contain the expected matter phase diagram, with in particular a critical Ising transition line meeting a first order line at a tricritical Ising transition point for some positive values of the activities $(z_1, z_2) = (z_1^{(t)}, z_2^{(t)})$. It also displays a line of Lee-Yang edge singularities terminating at a higher order critical point described by a non-unitary CFT with central charge $c(2, 7) = -68/7$ at some point $z_1 = z_1^{(t')} > 0$ and $z_2 = z_2^{(t')} < 0$. A few concluding remarks are gathered in Sect. 4, while additional technical derivations or more involved cases are left to appendices A-E.

2. Nearest neighbor exclusion models on regular and random lattices

In this section, we study generic models of nearest neighbor exclusion in which hard particles live on the vertices of either regular or random lattices. The exclusion rule simply states that when a vertex is occupied by a particle, all its nearest neighbors must be vacant. We first briefly recall known facts about the so-called “hard square” model of hard particles on the regular square lattice [5-7] and the corresponding model of hard particles on the regular honeycomb lattice [8]. As explained below, these models share the same qualitative phase diagram, where the structure of the ordered phase strongly relies on the vertex-bicolorability (i.e. the bipartite nature) of the underlying lattice. We then present an exact solution of the same models on random lattices. We first consider the case of arbitrary random graphs standardly used in the context of discretized 2D quantum gravity [9,10]. We note the disappearance of the ordered phase which can be traced back to the generic lack of vertex bicolorability of the graphs. We therefore study the case of vertex-bicolorable (or so-called Eulerian) random graphs, for which we derive the phase diagram in the planar limit. As expected, the ordered phase is reinstated in this case, and we find a continuous transition point in the universality class of the critical Ising model coupled to 2D quantum gravity.

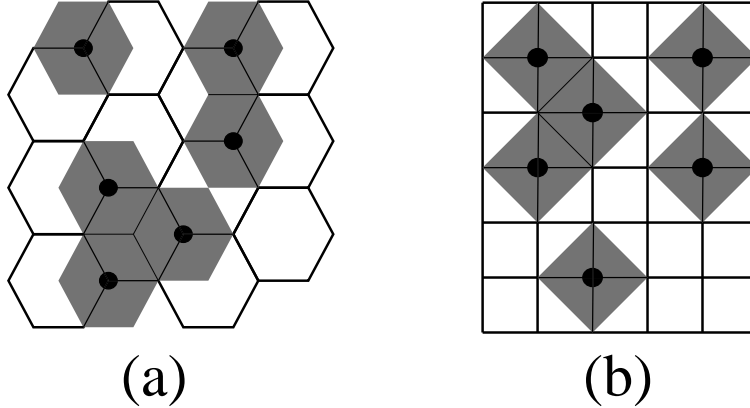


Fig. 1: Sample configurations of the hard particle model on the honeycomb (a) and square (b) lattices. The exclusion constraint between particles (represented as black dots) may be translated into a non-overlapping constraint for hard tiles, either hexagons (a) or squares (b).

2.1. Nearest neighbor exclusion on the square and honeycomb lattices

Let us consider nearest neighbor particle exclusion models on respectively the regular trivalent honeycomb lattice and regular tetravalent square lattice. Each particle comes with an activity z and excludes its nearest neighbors. A simple pictorial representation of the exclusion rule is to replace particles with non-overlapping hexagons, resp. squares, with centers on the vertices of the lattice, as depicted in Fig. 1. The phase diagrams of both models have been derived using numerical (corner) transfer matrix methods in [6,8]. They both display two critical points.

The first “non-physical” critical point occurs at a negative value z_- of the activity and corresponds to the so-called Lee-Yang edge singularity [11] (non-unitary CFT with central charge $c(2,5) = -22/5$), with the estimates $z_-^{(3)} = -0.15\dots$ (extracted from [5]) for the (trivalent) honeycomb lattice and $z_-^{(4)} = -0.122\dots$ [6] for the (tetravalent) square lattice. The values z_- of z at these critical points can be obtained from the singularity of the thermodynamic free energy $F(z)$ expressed as an alternating series in powers of z . For $z \xrightarrow{\sim} z_-$, the singular part of the free energy behaves as $F(z)|_{\text{sing}} \sim (z - z_-)^{2-\alpha}$ where $\alpha = 7/6$ is the thermal exponent predicted by the CFT. This apparently non-physical critical point with negative activity can be reinterpreted as a positive activity critical point at $t_+ = -z_-$ for heaps of hexagons, resp. squares with activity $t = -z$ per object in $2 + 1$ dimensions, with free energy $\Phi(t) = -F(z = -t)$ [12].

The second “physical” critical point occurs at a positive value z_+ and corresponds to a continuous transition between a low activity disordered fluid phase and a high activity

ordered crystalline phase where the hard particles condense preferably on one of the two sublattices of the lattice. Estimates for the critical points are $z_+^{(3)} = 7.92\dots$ [8] and $z_+^{(4)} = 3.7962\dots$ [6]. More precisely, the honeycomb and square lattice are bipartite lattices whose vertices can be naturally bicolored, say black and white, in such a way that a vertex of one color has only neighbors of the other. The corresponding order parameter $M = \rho_B - \rho_W$, which measures the difference of density of particles between the black and white sublattice, is zero in the fluid phase and non-zero in the crystalline one. Based on numerical evidence, it is commonly accepted that this transition lies in the universality class of the critical Ising model (CFT with $c(3,4) = 1/2$), with a thermal exponent $\alpha = 0$ and a magnetic exponent $\beta = 1/8$ corresponding to the singularity of the order parameter $M \sim (z - z_+)^{\beta}$ for $z \xrightarrow{\searrow} z_+$.

Note that the two above critical points are essentially different in nature. The Lee-Yang critical point is much more universal and does not rely on any particular geometrical feature of the lattice. It is also observed for hard particles on the triangular lattice (the so-called “hard-hexagon” model). On random lattices, it was first observed for the Hard Dimer model in [13] and, as we shall see, it will show in all the hard particle models studied throughout this paper. On the contrary, the universality of the crystallization point strongly relies on the bicolability of the underlying lattice. In the case of the triangular lattice for instance, one finds instead a crystallization point governed by the critical three-state Potts model (CFT with $c(5,6) = 4/5$), directly related to the tricolorability of the lattice. In the case of random graphs, we shall also find that the bicolability is crucial to recover the Ising crystallization point.

2.2. Nearest neighbor exclusion model on a random lattice

We now turn to the study of nearest neighbor exclusion models on random graphs. In this section we will concentrate on the case of hard particles living at the vertices of arbitrary random *tetravalent* graphs. We use the standard matrix integral method to generate all configurations of the exclusion model on all possible tetravalent fatgraphs, including a weight g per tetravalent vertex (empty or occupied), z per particle, and the usual weight N^{2-2h} for graphs of genus h . We will mainly be interested in the planar limit $N \rightarrow \infty$ that selects only graphs with the topology of the sphere $h = 0$. More precisely, the generating function reads

$$Z_N^{(4)}(g, z) = \int dA dB e^{-N \text{Tr} V(A, B)} \tag{2.1}$$

$$V(A, B) = -\frac{1}{2}A^2 + AB - g\frac{B^4}{4} - gz\frac{A^4}{4}$$

where A, B are Hermitian matrices with size $N \times N$, and the measure is normalized so that $Z_N^{(4)}(0, 0) = 1$. The Feynman diagrammatic expansion of (2.1) is readily seen to generate tetravalent graphs with two types of vertices, occupied ($A^4/4$, with weight gz) and empty ($B^4/4$ with weight g), and with the propagators given by the inverse of the quadratic part of V , namely:

$$V_{\text{quad}} = \frac{1}{2}(A, B) Q \begin{pmatrix} A \\ B \end{pmatrix} \quad \text{and} \quad \begin{pmatrix} \langle AA \rangle & \langle AB \rangle \\ \langle BA \rangle & \langle BB \rangle \end{pmatrix} \propto Q^{-1} = \begin{pmatrix} 0 & 1 \\ 1 & 1 \end{pmatrix} \quad (2.2)$$

hence $\langle B_{ij}B_{kl} \rangle = \delta_{il}\delta_{jk}/N$ and $\langle A_{ij}B_{kl} \rangle = \delta_{il}\delta_{jk}/N$ (for a general review on matrix models see [9,10] and references therein). The vanishing of the $\langle AA \rangle$ propagator clearly enforces the exclusion rule.

To compute (2.1), we apply the standard technique of bi-orthogonal polynomials [9]. We introduce the monic bi-orthogonal polynomials p_n, q_m with respect to the scalar product $(f, g) = \int dx dy e^{-NV(x,y)} f(x)g(y)$, satisfying

$$(p_n, q_m) = h_n \delta_{n,m} \quad (2.3)$$

where the “norms” h_n are fully determined by the requirement that the polynomial p_n be monic of degree n . Introducing $h_n^{(0)} = h_n(g = 0, z = 0)$, and after reduction of (2.1) to an eigenvalue integral, we may rewrite [9]

$$Z_N^{(4)}(g, z) = \prod_{n=0}^{N-1} \frac{h_n}{h_n^{(0)}} \quad (2.4)$$

which reduces the computation of the partition function to that of the h_n 's.

We introduce the operators of multiplication by eigenvalues Q_1 and Q_2 , expressed on the orthogonal polynomials as $Q_1 p_n(x) = x p_n(x)$ and $Q_2 q_m(y) = y q_m(y)$, and the operators of derivation with respect to eigenvalues P_1 and P_2 expressed as $P_1 p_n(x) = p_n'(x)$, $P_2 q_m(y) = q_m'(y)$. Integrating by parts, we get the system of equations

$$\begin{aligned} (P_1 p_n, q_m) &= N \left(\frac{\partial}{\partial x} V(x, y) p_n(x), q_m(y) \right) = N(p_n, Q_2 q_m) - N((Q_1 + gz Q_1^3) p_n, q_m) \\ (p_n, P_2 q_m) &= N \left(\frac{\partial}{\partial y} V(x, y) p_n(x), q_m(y) \right) = N(Q_1 p_n, q_m) - N g (p_n, Q_2^3 q_m) \end{aligned} \quad (2.5)$$

Note that $Q_1 p_n$ is a linear combination of the p_j 's for $0 \leq j \leq n+1$, and similarly for $Q_2 q_m$, combination of the q_i 's for $0 \leq i \leq m+1$, while $P_1 p_n$ is a linear combination of the p_j 's for $0 \leq j \leq n-1$ and similarly $P_2 q_m$, combination of the q_i 's for $0 \leq i \leq m-1$.

From orthogonality, we see that for $m > n + 3$ in the first line of (2.5) and for $m < n - 3$ in the second, we get respectively that $(p_n, Q_2 q_m) = 0$ and $(Q_1 p_n, q_m) = 0$. Hence the linear combinations reduce respectively to finite ranges of indices $n - 3 \leq j \leq n + 1$ and $m - 3 \leq i \leq m + 1$. Moreover, from the parity of the potential $V(x, y) = V(-x, -y)$, we deduce the parity of the polynomials: $p_n(x) = (-1)^n p_n(-x)$ and $q_m(y) = (-1)^m q_m(-y)$. So finally the action of Q_1 and Q_2 takes the form

$$\begin{aligned} Q_1 p_n(x) &= p_{n+1}(x) + r_n p_{n-1}(x) + s_n p_{n-3}(x) \\ Q_2 q_m(y) &= q_{m+1}(y) + \tilde{r}_m q_{m-1}(y) + \tilde{s}_m q_{m-3}(y) \end{aligned} \quad (2.6)$$

The fact that Q_1 and Q_2 have a finite range is generic of multimatrix models with polynomial interactions. Eqns. (2.5) and (2.6) can be expressed in an operatorial way. Introducing the adjoint operators Q_1^\dagger and Q_2^\dagger with respect to the above scalar product, eqn. (2.5) takes the form:

$$\begin{aligned} \frac{P_1}{N} &= Q_2^\dagger - Q_1 - g z Q_1^3 \\ \frac{P_2}{N} &= Q_1^\dagger - g Q_2^3 \end{aligned} \quad (2.7)$$

Let us introduce the shift operators σ, τ acting respectively on the p 's and q 's as $\sigma p_n = p_{n+1}$, $\tau q_n = q_{n+1}$ and their adjoints $\sigma^\dagger, \tau^\dagger$, such that

$$\sigma^\dagger = \tau^{-1} v \quad \tau^\dagger = \sigma^{-1} v \quad (2.8)$$

where $v = v^\dagger$ is the diagonal operator acting as $v p_n = v_n p_n$ and $v q_n = v_n q_n$, with

$$v_n = \frac{h_n}{h_{n-1}} \quad (2.9)$$

Analogously we define the diagonal operators $\nu, r, s, \tilde{r}, \tilde{s}$ acting on p_n and q_n respectively as the multiplication by $n, r_n, s_n, \tilde{r}_n, \tilde{s}_n$. In terms of these operators, the P and Q operators read finally

$$\begin{aligned} Q_1 &= \sigma + \sigma^{-1} r + \sigma^{-3} s \\ Q_2 &= \tau + \tau^{-1} \tilde{r} + \tau^{-3} \tilde{s} \\ Q_1^\dagger &= \tau^{-1} v + r v^{-1} \tau + s (v^{-1} \tau)^3 \\ Q_2^\dagger &= \sigma^{-1} v + \tilde{r} v^{-1} \sigma + \tilde{s} (v^{-1} \sigma)^3 \\ P_1 &= \sigma^{-1} \nu + O(\sigma^{-3}) \\ P_2 &= \tau^{-1} \nu + O(\tau^{-3}) \end{aligned} \quad (2.10)$$

To obtain a system of recursion relations involving the sequence $v_n = h_n/h_{n-1}$, let us now write order by order in τ and σ the two relations (2.7):

$$\begin{aligned}
O(\sigma^{-1}) : \sigma^{-1} \frac{\nu}{N} &= \sigma^{-1}(v-r) - gz(r\sigma^{-1}r + \sigma^{-1}r^2 + (\sigma^{-1}r)^2\sigma + \sigma^{-1}s + \sigma^{-2}s\sigma + \sigma^{-3}s\sigma^2) \\
O(\sigma) : 0 &= \tilde{r}v^{-1}\sigma - \sigma - gz(\sigma r + r\sigma + \sigma^{-1}r\sigma^2) \\
O(\sigma^3) : 0 &= \tilde{s}(v^{-1}\sigma)^3 - gz\sigma^3
\end{aligned} \tag{2.11}$$

and

$$\begin{aligned}
O(\tau^{-1}) : \tau^{-1} \frac{\nu}{N} &= \tau^{-1}v - g(\tilde{r}\tau^{-1}\tilde{r} + \tau^{-1}\tilde{r}^2 + (\tau^{-1}\tilde{r})^2\tau + \tau^{-1}\tilde{s} + \tau^{-2}\tilde{s}\tau + \tau^{-3}\tilde{s}\tau^2) \\
O(\tau) : 0 &= rv^{-1}\tau - g(\tau\tilde{r} + \tilde{r}\tau + \tau^{-1}\tilde{r}\tau^2) \\
O(\tau^3) : 0 &= s(v^{-1}\tau)^3 - g\tau^3
\end{aligned} \tag{2.12}$$

It is not difficult to check that the first lines of (2.11) and (2.12) are equivalent modulo the other equations, so that we are left with five equations for the five unknown sequences $v_n, r_n, s_n, \tilde{r}_n, \tilde{s}_n$.

The planar (genus zero) limit of these equations amounts to taking $n, N \rightarrow \infty$ with $x = n/N$ fixed, in which case all sequences converge to functions of x . More precisely, we define the rescaled limits $V(x), R(x), S(x), \tilde{R}(x), \tilde{S}(x)$ of respectively $gv_n, gr_n, g^2s_n, g\tilde{r}_n, g^2\tilde{s}_n$. These functions are determined by rewriting (2.11) and (2.12) in this limit which amounts to treating all operators as scalars (in particular $\sigma = \tau = 1$), with the result

$$\begin{aligned}
gx &= V - R - 3z(R^2 + S) \\
0 &= \tilde{R} - V(1 + 3zR) \\
0 &= \tilde{S} - zV^3 \\
0 &= R - 3V\tilde{R} \\
0 &= S - V^3
\end{aligned} \tag{2.13}$$

After substitutions, this reduces to

$$gx = \varphi(V) \equiv V(1 - 3zV^2) - \frac{3V^2}{(1 - 9zV^2)^2} \tag{2.14}$$

For fixed g and z this equation defines upon inversion the function $V(x)$ encoding the asymptotic properties of the sequence v_n , hence those of the h_n 's. More precisely, using

eqn. (2.4), the thermodynamic free energy in the planar limit reads

$$\begin{aligned} f_0^{(4)}(g, z) &= - \lim_{N \rightarrow \infty} \text{Log}(Z_N^{(4)}(g, z))/N^2 \\ &= - \int_0^1 dx (1-x) \text{Log} \left(\frac{V(x)}{gx} \right) \end{aligned} \quad (2.15)$$

where the normalization gx in the logarithm ensures the correct normalization of the partition function, namely $f_0^{(4)}(g=0, z=0) = 0$. For g sufficiently small, eqn. (2.14) determines a unique solution $V(x)$ which is monotonous and such that $V(x) \sim gx$ for small x . To compute $f_0^{(4)}(g, z)$, we must substitute this solution into (2.15) and perform the integration. It is natural to perform the change of variables $x \rightarrow V$, which yields

$$f_0^{(4)}(g, z) = \int_0^{V_{g,z}} dV \frac{\varphi'(V)}{g} \left(1 - \frac{\varphi(V)}{g} \right) \text{Log} \left(\frac{\varphi(V)}{V} \right) \quad (2.16)$$

where $V_{g,z}$ is the value of V at $x = 1$, satisfying $\varphi(V_{g,z}) = g$ for fixed g and z . The singularities of the planar free energy are due to those of $V_{g,z}$ as a function of g and z . For fixed z , the first singularity of $f_0^{(4)}(g, z)$ is attained at a critical value $g = g_c(z)$, where the value $V_c(z) \equiv V_{g_c(z), z}$ is such that $\varphi'(V_c(z)) = 0$. In the vicinity of this point, (2.14) reduces to $g_c(z) - g \sim (V_c(z) - V_{g,z})^2$, which in turn yields a generic square root singularity for $V_{g,z}$ in (2.15). To get the corresponding singularity of the free energy, we note that, taking successive derivatives of (2.16) with respect to g and using $\varphi(V_{g,z}) = g$, we simply get the general formula

$$\frac{d^2}{dg^2} g^3 \frac{d}{dg} f_0^{(4)}(g, z) = 1 - \frac{g}{V_{g,z}} \frac{dV_{g,z}}{dg} \quad (2.17)$$

The square root singularity of $V_{g,z}$ immediately translates into a string susceptibility exponent γ , defined by $f_0^{(4)}(g, z)|_{\text{sing}} \sim (g_c(z) - g)^{2-\gamma}$, with value $\gamma = -1/2$. The critical value $g_c(z)$ also corresponds to the maximum value of g for which the series expansion of the free energy converges.

Writing $g_c(z) = \varphi(V_c(z))$ and $0 = \varphi'(V_c(z))$ yields parametric equations for the critical line $g_c(z)$, in terms, say, of the parameter $u = 3zV_c(z)^2$:

$$z = \frac{12u(1+3u)^2}{(1-3u)^8} \quad g_c(z) = \frac{(1-3u)^4(1+10u-15u^2)}{12(1+3u)^2} \quad (2.18)$$

This line is plotted in Fig.2. The solid curve corresponds to the true critical values of $g = g_c(z)$, corresponding to a first maximum of $\varphi(V)$, while the dashed line corresponds

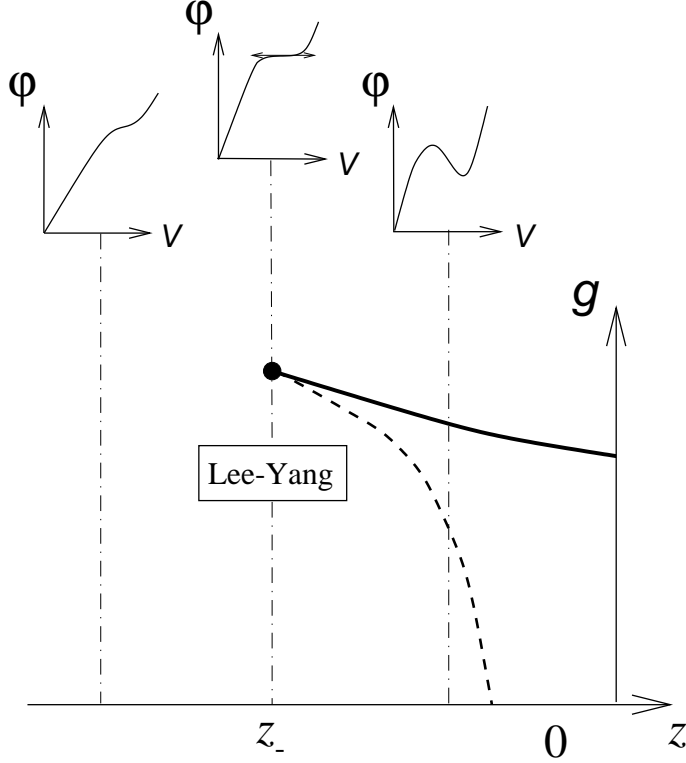


Fig. 2: Critical line $g_c(z)$ for the hard particle model on arbitrary random lattices, as obtained by setting $\varphi'(V) = 0$. The solid line represents the true critical values of $g = g_c(z)$ corresponding to the maximum of φ first attained by the change of variable $x \rightarrow V$, while the dashed line corresponds to a further minimum as displayed on the top right plot of the figure. These extrema merge at the Lee-Yang critical point z_- where $\varphi''(V) = 0$ (top center plot) and disappear from the real plane (by becoming complex) for $z < z_-$ (top left plot).

to a further minimum of $\varphi(V)$ which is never attained by the above change of variables. The solid line stops at a finite negative value of z below which $g_c(z)$ becomes complex. We note that for $z = 0$ ($u = 0$) we recover the critical value $g_c = 1/12$ for pure arbitrary tetravalent graphs [14]. The solid and dashed lines merge into a cusp at a higher order critical point satisfying in addition $\varphi''(V) = 0$, as it corresponds to the coalescence of the maximum and the minimum of φ (see Fig.2). This point corresponds to the values

$$\begin{aligned}
 z_- &= -\frac{25}{8192}(11\sqrt{5} + 25) = -0.151\dots \\
 g_- &= g_c(z_-) = \frac{64}{45}(13\sqrt{5} - 29) = 0.0979\dots \\
 V_- &= V_c(z_-) = 32/75(7\sqrt{5} - 15) = 0.278\dots
 \end{aligned}
 \tag{2.19}$$

At this point, the above scaling argument now becomes $g_- - g \sim (V_- - V)^3$, hence translates directly into a string susceptibility exponent $\gamma = -1/3$. As the critical activity

z_- is negative, we identify this higher critical point with the unique non-unitary theory with $\gamma = -1/3$, namely the Lee-Yang edge singularity with $c(2, 5) = -22/5$, coupled to 2D quantum gravity (see Appendix A). This identification may be corroborated in two different ways. On one hand, one may compute the thermal exponent α which measures the singularity of the free energy at the critical point as a function of z , and compare it to the predicted value $\alpha = 1/2$ for the Lee-Yang edge singularity coupled to 2D quantum gravity, as re-derived in Appendix A below. Writing the thermodynamic free energy per site as $f^{(4)}(z) = -\lim_{A \rightarrow \infty} \frac{1}{A} \text{Log } Z_A(z)$ where $Z_A(z)$ is the partition function for planar graphs of fixed number of vertices (area) A , we read α from the singular part $f^{(4)}(z)|_{\text{sing}} \sim (z - z_-)^{2-\alpha}$. Using $f^{(4)}(z) = \text{Log } g_c(z)$, α may be obtained by computing the singular part of $g_c(z)$. Expanding eqn. (2.18) in powers of $u - u_-$, we find that $g_c(z) - g_- = a(u - u_-)^2 + b(u - u_-)^3 + \dots$ and $z - z_- = a'(u - u_-)^2 + b'(u - u_-)^3 + \dots$ with $u_- = 3z_- V_-^2$, and which, upon inversion, yields $g_c(z) - g_- = a''(z - z_-) + b''(z - z_-)^{\frac{3}{2}} + \dots$ with a non-vanishing value of b'' . Hence we get $2 - \alpha = 3/2$ as expected. On the other hand, one may also derive the so-called double scaling limit of the model at the critical point and write a differential equation for the renormalized string susceptibility, easily identified with that of the Lee-Yang edge singularity coupled to 2D quantum gravity. This derivation is presented in Appendix B below.

Note that for $z < z_-$, the gravitational critical value of g becomes complex with $g_c(z) = \rho e^{i\theta}$, but it still governs the large area behavior of the above partition function $Z_A(z)$ which now oscillates typically as

$$Z_A(z) \sim \rho^{-A} \cos(A\theta) \tag{2.20}$$

which allows to identify the thermodynamic free energy as $\text{Log } \rho$.

In conclusion, when comparing with the regular lattice results, we see that the naive gravitational version of the exclusion model fails to reproduce the crystallization transition, and leaves us only with the “non-physical” Lee-Yang edge singularity. As shown in Appendix C, the case of trivalent graphs instead of tetravalent is exactly solvable as well and displays the same structure. The absence of a crystalline ordered phase should not come as a surprise, as the partition function involves a sum over graphs that are not generically bicolourable, hence do not allow for a canonical crystalline order, where half of the vertices are preferentially occupied. To emphasize the role played by bicolourability for exclusion models, we note that for large z ($u \rightarrow 1/3$ in eqn. (2.18)) the quantity $\sqrt{z} g_c(z)$ tends to

2/9, which is precisely the critical value of g in a model of pure bicolored tetravalent graphs⁴. This clearly shows that in this limit the selected configurations are half-occupied vertex-bicolored graphs.

To recover a crystallization transition at finite z , we shall consider in the next section the coupling of exclusion models to Eulerian gravity.

2.3. Nearest neighbor exclusion models on vertex-bicolored random lattices

In this section, we consider a restricted gravitational version of the nearest neighbor exclusion model, in which we explicitly sum only over the so-called random Eulerian graphs, simply defined as vertex-bicolored (or bipartite) graphs. It turns out that the case of trivalent Eulerian graphs is technically simpler than that of tetravalent ones, yet it displays the same qualitative physical behavior. Therefore we will now concentrate on the trivalent case and leave the tetravalent one to Appendix E.

The configurations of the nearest neighbor exclusion model on Eulerian trivalent graphs are again generated by a matrix model replacing (2.1). We now need a total of four matrices, as the vertices must be bicolored and empty or occupied. More precisely, we use a matrix A_1 (resp. A_4) for empty black (resp. white) vertices and a matrix A_2 (resp. A_3) for occupied white (resp. black) vertices. The resulting matrix model reads

$$Z_N^{(3)}(g, z) = \int dA_1 dA_2 dA_3 dA_4 e^{-N \text{Tr} V(A_1, A_2, A_3, A_4)} \quad (2.21)$$

$$V(A_1, A_2, A_3, A_4) = A_1 A_2 - A_2 A_3 + A_3 A_4 - g \left(\frac{A_1^3}{3} + \frac{A_4^3}{3} \right) - gz \left(\frac{A_2^3}{3} + \frac{A_3^3}{3} \right)$$

The quadratic form in $V(A_1, A_2, A_3, A_4)$ has been engineered so as to reproduce the correct propagators, namely that only black and white vertices are connected in the Feynman diagrams ($\langle A_i A_j \rangle = 0$ if i and j have the same parity) and that two occupied neighboring vertices exclude one-another ($\langle A_2 A_3 \rangle = 0$).

Due to the chain-like interaction between the matrices, this model turns out to be solvable by means of bi-orthogonal polynomials. In addition the symmetry $A_i \leftrightarrow A_{5-i}$ implies that the two sets of polynomials are identical. We therefore introduce the monic

⁴ This critical value was computed in [15] in the context of a particular $O(n=1)$ gravitational model.

polynomials p_n , orthogonal with respect to the appropriate symmetric scalar product, namely

$$(p_n, p_m) = \int dx_1 dx_2 dx_3 dx_4 e^{-NV(x_1, x_2, x_3, x_4)} p_n(x_1) p_m(x_4) = h_n \delta_{n,m} \quad (2.22)$$

As before, we introduce operators Q_i of multiplication by x_i , $i = 1, 2, 3, 4$ but this time all acting on $p_n(x_1)$, but the symmetry $A_i \leftrightarrow A_{5-i}$ immediately implies that $Q_3 = Q_2^\dagger$ and $Q_4 = Q_1^\dagger$. We also introduce the operator P_1 acting on $p_n(x_1)$ as d/dx_1 . These operators satisfy the system

$$\begin{aligned} \frac{P_1}{N} &= Q_2 - gQ_1^2 \\ Q_1 &= Q_2^\dagger + gzQ_2^2 \end{aligned} \quad (2.23)$$

obtained by integrating by parts.

To write explicitly the action of Q_1 and Q_2 on the p_n 's, let us first notice that the potential V satisfies the symmetry relation

$$V(\omega x_1, \omega^2 x_2, \omega x_3, \omega^2 x_4) = V(x_1, x_2, x_3, x_4), \quad \omega = e^{2i\pi/3} \quad (2.24)$$

This translates into the symmetry relation for the monic orthogonal polynomials

$$\omega^{2n} p_n(\omega x) = p_n(x) \quad (2.25)$$

Now from (2.23) it is easy to show that Q_1 and Q_2 have finite range, and more precisely, thanks to the symmetry relation (2.25)

$$\begin{aligned} Q_1 &= \sigma + \sigma^{-2} r^{(1)} + \sigma^{-5} r^{(2)} + \sigma^{-8} r^{(3)} \\ Q_2 &= \sigma^2 s^{(0)} + \sigma^{-1} s^{(1)} + \sigma^{-4} s^{(2)} \end{aligned} \quad (2.26)$$

where σ is the shift operator acting on the p 's as $\sigma p_n = p_{n+1}$ and the operators $r^{(i)}, s^{(i)}$ are diagonal. Introducing as before the diagonal operator v with entries $v_n = h_n/h_{n-1}$, we have $\sigma^\dagger = \sigma^{-1}v$, and therefore

$$Q_2^\dagger = s^{(0)}(\sigma^{-1}v)^2 + s^{(1)}v^{-1}\sigma + s^{(2)}(v^{-1}\sigma)^4 \quad (2.27)$$

Expanding the relations (2.23) order by order in σ , we finally arrive at

$$\begin{aligned} s^{(0)} &= g \\ s^{(2)} &= -g^3 z \sigma^4 (\sigma^{-1}v)^4 \\ v &= s^{(1)} + g^2 z v (\sigma s^{(1)} \sigma^{-1} + \sigma^{-1} s^{(1)} \sigma) \\ r^{(1)} &= g \sigma v \sigma^{-1} v + g z \sigma s^{(1)} \sigma^{-1} s^{(1)} + g^2 z (s^{(2)} + \sigma^{-2} s^{(2)} \sigma^2) \\ \frac{\nu}{N} &= s^{(1)} - g(r^{(1)} + \sigma^{-1} r^{(1)} \sigma) \end{aligned} \quad (2.28)$$

where ν is the diagonal operator with entries n .

In the planar limit, we express the system (2.28) in terms of the rescaled limiting functions $S(x) = \lim g^2 z s^{(1)}$, $V(x) = \lim g^2 z v$, where $x = n/N$ while $n, N \rightarrow \infty$, and also use the fact that $\sigma \rightarrow 1$. The third line of (2.28) allows to solve for $S = V/(1 + 2V)$, so that we finally get

$$g^2 z^2 x \equiv \varphi(V) = z \frac{V}{(1 + 2V)^2} - 2V^2(1 - 2V^2) \quad (2.29)$$

Writing

$$\varphi'(V) = \frac{(1 - 2V)(z - 4V(1 + 2V)^4)}{(1 + 2V)^3} = 0 \quad (2.30)$$

we get two candidates for the critical line, namely $V = 1/2$ or $z = 4V(1 + 2V)^4$.

These lead respectively to the two possible critical curves $g^2(z) = \varphi(V)/z^2$ parametrized by

$$\begin{aligned} g_1^2(z) &= \frac{1}{8z} - \frac{1}{4z^2}, \quad z > 0, \quad V = 1/2 \\ g_2^2(z) &= \frac{1 + 8V + 10V^2}{8(1 + 2V)^8}, \quad \text{with } z(V) = 4V(1 + 2V)^4 \end{aligned} \quad (2.31)$$

where the condition $z > 0$ in the first line simply follows from the positivity requirement for the norm ratios v_n , implying that V and z have the same sign.

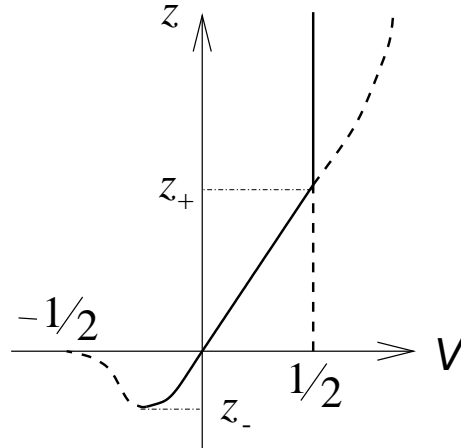


Fig. 4: Critical lines in the (V, z) plane as obtained by setting $\varphi'(V) = 0$. The correct line corresponds to the lowest value of $|V|$ and is represented by a solid line. The Lee-Yang critical point z_- is characterized by $dz/dV = 0$ and corresponds to the merging and annihilation of two extrema. The Ising critical point z_+ corresponds to the crossing of two determinations of $V(z)$.

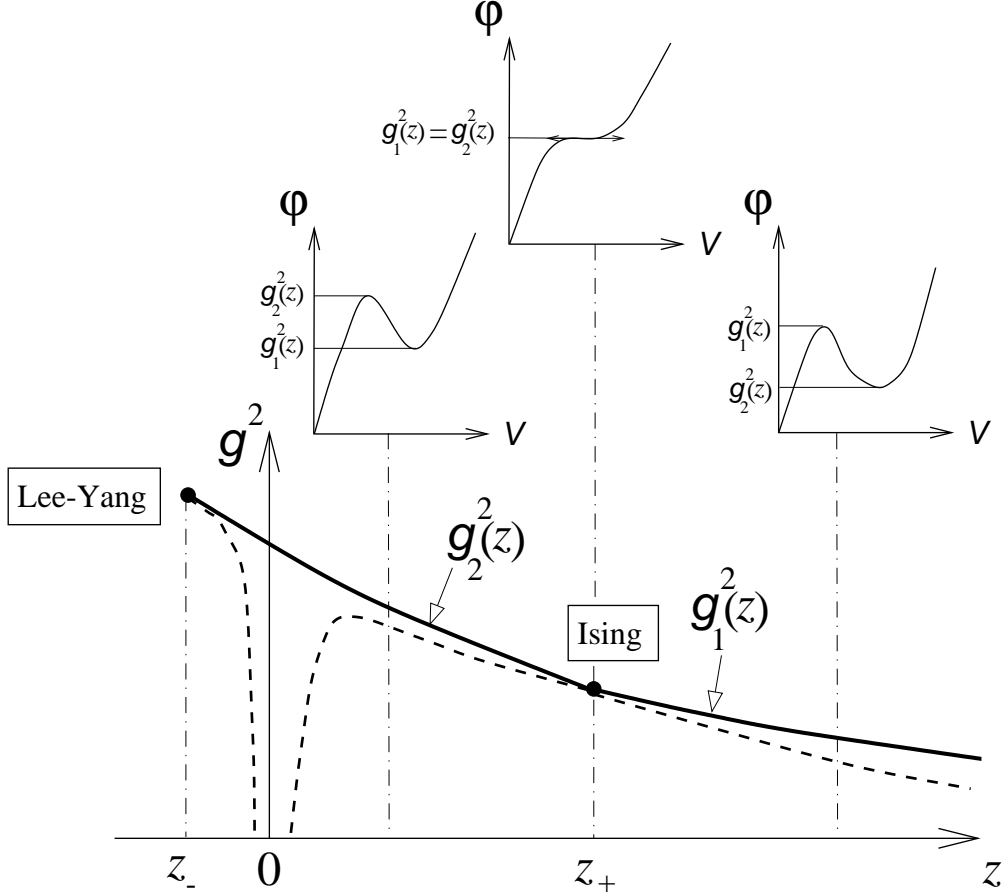


Fig. 3: Critical line $g_c(z)$ for the hard particle model on vertex bicolored random lattices, as obtained by setting $\varphi'(V) = 0$. The solid line represents the true critical values of $g = g_c(z)$ corresponding to the maximum of φ first attained by the change of variable $x \rightarrow V$, while the dashed line corresponds to a further minimum as displayed on the top plots. The curve terminates at a Lee-Yang critical point similar to that of Fig. 2. The maximum and minimum swap determinations at the critical Ising point z_+ where $\varphi''(V) = 0$ (top center plot).

These two lines are represented in Fig.3. The choice of the correct determination in (2.31) is best seen by plotting the critical lines in a (V, z) diagram as in Fig. 4. In this picture, the correct singularity of the free energy at fixed z is always given by the lowest critical value of $|V|$ as it is the one attained by the above change of variables. The true critical points of the free energy are represented by solid pieces of curves in Fig. 3, and correspond to maxima of $\varphi(V)$, while the dashed parts correspond to further minima of $\varphi(V)$ never attained by the change of variables as before. Along these lines the string susceptibility exponent is $\gamma = -1/2$. We note that for $z = 0$, we recover the critical value $g_c^2 = 1/8$ for pure bicolored trivalent graphs [16,17]. Also for $z \rightarrow \infty$ we get

$g^2(z) = g_1^2(z) \sim 1/(8z)$ as expected for half-occupied trivalent bicolored graphs.

The higher order critical points correspond to the cuspidal singularity at z_- , where the maximum and minimum of $\varphi(V)$ merge and annihilate each other, and to the crossing between the two curves at z_+ , where the value of the maximum of φ hops from $g_2(z)$ to $g_1(z)$ while its minimum hops from $g_1(z)$ to $g_2(z)$. The position of these points is obtained by writing the extra condition $\varphi''(V) = 0$, with

$$\varphi''(V) = \begin{cases} \frac{32-z}{4} & \text{if } V = 1/2 \\ 4(2V-1)(1+10V) & \text{if } z = 4V(1+2V)^4 \end{cases} \quad (2.32)$$

We get the two critical values

$$\begin{aligned} (1) \quad V_+ &= \frac{1}{2}, & z_+ &= 32, & g_+^2 &= \frac{15}{2^{12}} \\ (2) \quad V_- &= -\frac{1}{10}, & z_- &= -\frac{2^9}{5^5}, & g_-^2 &= \frac{3 \cdot 5^7}{2^{20}} \end{aligned} \quad (2.33)$$

The critical point z_- is similar to that of Sect. 2.2 and corresponds to the Lee-Yang edge singularity. The crucial outcome of our calculation is the emergence of a crystalline phase at finite values of z , with a crystallization transition at z_+ . This critical point turns out to be in the universality class of the critical Ising model on random graphs. The simplest reason for these identifications is that both above critical points have string susceptibility exponent $\gamma = -1/3$ by construction, and that only two CFT's are candidates to describe this⁵, the Lee-Yang edge singularity with $c(2, 5) = -22/5$ which is non-unitary as expected for a negative value $z = z_-$, and the critical Ising model with $c(3, 4) = 1/2$ which is a unitary theory, as expected for a positive critical activity z_+ . To further confirm the identification of the critical Ising universality class, one can compute the thermal exponent α for the crystallization transition. It is easy to see from the above formulas that the transition from the curve $g_1(z)$ to $g_2(z)$ is continuous at z_+ , with continuous first and second derivative, and with a discontinuity of the third one. This gives a thermal exponent $\alpha = -1$, as expected for the critical Ising model coupled 2D quantum gravity (see Appendix A). We have also derived the differential equations for the string susceptibility for both cases in the corresponding double scaling limits, and identified them with the known results for the Lee-Yang and Ising critical models coupled to 2D quantum gravity. The details of these calculations are given in Appendix D below.

⁵ Indeed for a CFT with central charge $c(p, q) = 1 - 6(p-q)^2/(pq)$, we have $\gamma = -2/(p+q-1)$, hence here $p+q = 7$, and $(p, q) = (2, 5), (3, 4)$ only.

3. Two-particle exclusion models on regular and random lattices

In this section, we extend our analysis of exclusion models on bicolored lattices to incorporate the physics of higher order critical points. More precisely, in the previous section we have reproduced the universality class of the critical Ising model within the context of exclusion models on bicolored random graphs. The crucial feature leading to the Ising symmetry is the existence of two degenerate symmetric crystalline groundstates playing the role of the two (up and down) ferromagnetic groundstates.

We now wish to construct in the language of particle exclusion a model reproducing the physics of the tricritical Ising model. In the framework of spin systems, the latter is found for instance in the phase diagram of a dilute Ising model, with spins $\sigma = 0, \pm 1$ [18], where the spins $\sigma = 0$ play the role of annealed non-magnetic vacancies. The existence of a tricritical point is associated to that of three non-symmetric groundstates of constant spin: the two groundstates $\sigma = +1$ and $\sigma = -1$ play symmetric roles, but $\sigma = 0$ is on a different footing. The Ising second order phase transition in the absence of vacancies extends into a line of second order transition points for low enough activity per vacancy. On the other hand, at low enough temperature, a first order transition line separates a ferromagnetic phase at low activity per vacancy from a paramagnetic phase at large activity per vacancy. Both lines merge at a tricritical point whose behavior defines the tricritical Ising universality class (CFT with $c(4, 5) = 7/10$). (For a general review on tricritical points in the context of spin systems or lattice gases see [19].)

In the next section, we show how to realize a similar behavior within the framework of hard objects, by use of a *two-particle* nearest neighbor exclusion model. We first describe its expected phase diagram on a regular bicolored lattice. Here again, the bicoloredness of the underlying lattice is crucial for the existence of an ordered crystalline phase. We then derive an exact solution of the same model on bicolored random lattices and recover the expected phase diagram, with in particular a tricritical point coupled to 2D quantum gravity.

3.1. Two-particle nearest neighbor exclusion models on the square and honeycomb lattices

In its simplest formulation, the two-particle exclusion model we wish to study is defined by putting particles on the vertices of a regular bicolored lattice (typically square or honeycomb), with the exclusion rule that a total of at most two particles may occupy the two vertices adjacent to any edge. In particular, we allow for two particles to occupy

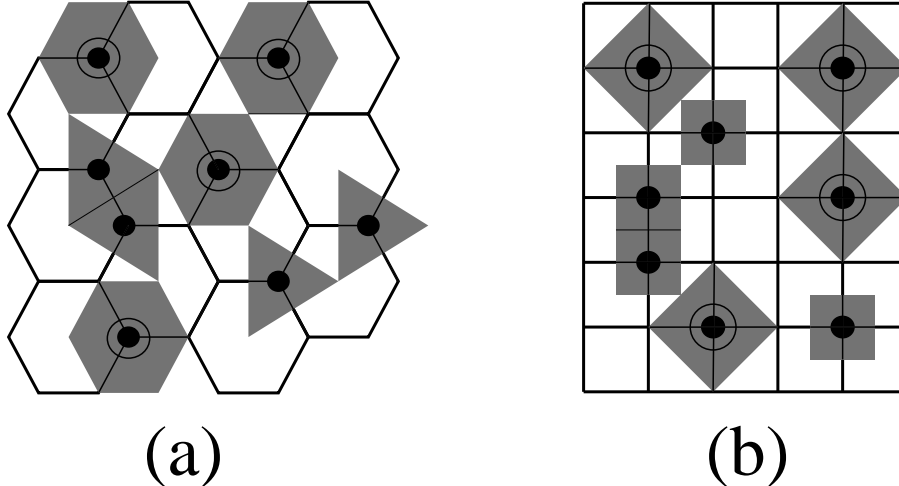


Fig. 5: Sample configurations of the two-particle exclusion model on the honeycomb (a) and square (b) lattices. The black dots represent singly occupied vertices while the circled black dots represent doubly occupied vertices. The two-particle exclusion constraint that an edge be shared by at most two particles may be translated into a non-overlapping constraint for hard tiles, either hexagons for double occupancy and triangles for single occupancy (a) or big tilted squares for double occupancy and small squares for single occupancy (b).

the same vertex, in which case its nearest neighbors must be vacant, while singly occupied vertices may be nearest neighbors. We assign a weight z_1 for singly occupied vertices and a weight z_2 for doubly occupied ones, with typically $u = z_2/z_1^2$ measuring the attractive ($u > 1$) or repulsive ($u < 1$) interaction between particles on the same vertex. As in the one-particle models of Sect. 2, we may represent pictorially the exclusion constraint in terms of non-overlapping hard objects on the corresponding lattices. As shown in Fig. 5, for the square lattice, doubly occupied sites may be represented as usual hard squares, which exclude their four neighbors, while singly occupied sites are represented by a new type of squares which are twice as small and may thus occupy two neighboring sites. Similarly, for the honeycomb lattice, we represent doubly and singly occupied vertices respectively by hard hexagons and triangles that are twice as small.

In both cases, we have three crystalline groundstates corresponding to a maximal covering of the lattice: two of them are symmetric and use only the larger tiles which occupy one of the two sublattices of the bipartite lattice, the third one is obtained by tiling the lattice with the smaller objects. The phase diagram of the model is best represented in the variables $(1/z_2, u^{-1} = z_1^2/z_2)$ (see Fig. 6). On the axis $u^{-1} = 0$ (i.e. $z_1 = 0$), we recover the one-particle exclusion models of Sect. 2 with $z = z_2$, and in particular a

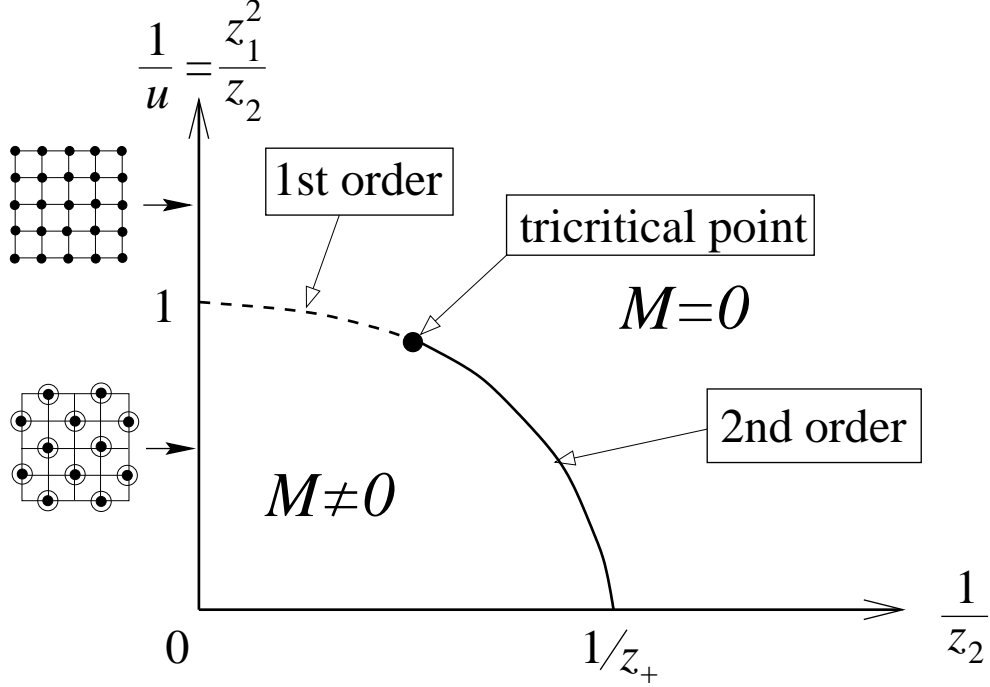


Fig. 6: Expected phase diagram in the $(1/z_2, u^{-1} = z_1^2/z_2)$ plane for positive activities. The ordered phase $M \neq 0$ corresponds to a crystallization of the doubly occupied vertices on one of the two mutually excluding sub-lattices. This phase is separated from the fluid phase $M = 0$ by a second order critical line for small enough u^{-1} and by a first order transition line for small enough $1/z_2$. Both lines are expected to meet at a tricritical point. The three natural groundstates in the problem are recovered along the axis $1/z_2 = 0$: for $u^{-1} < 1$ the two maximally filled doubly occupied configurations dominate (tilings with the bigger tiles) while at $u^{-1} > 1$, the full occupation by single particles (tiling with smaller tiles) dominates. The latter groundstate degenerates into a disordered fluid phase as soon as $1/z_2 > 0$.

crystallization point at $z_2 = z_+$. For fixed small enough u^{-1} , we expect a similar second order transition at some $z_2 = z_+(u)$. The critical curve $z_2 = z_+(u)$ separates the liquid phase from the crystal phase, the latter being characterized by the non-vanishing of the order parameter $M = \rho_B^{(2)} - \rho_W^{(2)}$ expressing the difference of densities of doubly occupied sites of either color. On the other hand, on the axis $(1/z_2) = 0$, i.e. $z_2 \rightarrow \infty$ and $z_1 \rightarrow \infty$, with $u^{-1} = z_1^2/z_2$ fixed, we have a competition between the three groundstates of maximal occupation. The two symmetric groundstates made of larger tiles have free energy per site $(\text{Log } z_2)/2$, while the other groundstate made of smaller tiles has free energy $\text{Log } z_1$. This leads to a first order transition at $u = 1$, with same order parameter $M = \pm 1$ for $u > 1$ and $M = 0$ for $u < 1$. We expect this transition point to extend into a first order transition

curve for small enough ($1/z_2$). By analogy with the tricritical Ising model phase diagram, we expect the two curves to meet at a tricritical point with $c(4, 5) = 7/10$.

These models do not seem to be simply solvable by integrable techniques, and the above phase diagram is somewhat conjectural. However, in the following section we shall present an exact solution of the random bicolored lattice version of the two-particle exclusion model, and show that it displays precisely the physical picture described above.

3.2. Two-particle exclusion model on vertex-bicolorable random lattices

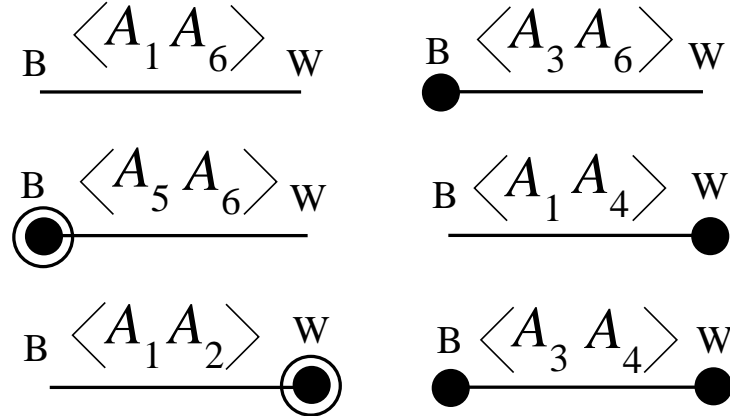


Fig. 7: The non-vanishing propagators corresponding to the six-matrix model generating the configurations of the two-particle exclusion model on vertex bicolorable random lattices. Identifying respectively A_1, A_3, A_5 with empty, singly occupied and doubly occupied black vertices on one hand and A_6, A_4, A_2 with empty, singly occupied and doubly occupied white vertices, the selected propagators enforce both the bicoloring constraint (black vertices are connected to white vertices only and conversally) and the exclusion constraint (at most two particles may share the same edge).

We start with the matrix model

$$\begin{aligned}
 Z_N(g, z_1, z_2) &= \int \prod_{i=1}^6 dA_i e^{-N \text{Tr} V(A_1, A_2, A_3, A_4, A_5, A_6)} \\
 V(A_1, A_2, A_3, A_4, A_5, A_6) &= A_1 A_2 - A_2 A_3 + A_3 A_4 - A_4 A_5 + A_5 A_6 \\
 &\quad - g \left(\frac{A_1^3}{3} + \frac{A_6^3}{3} \right) - g z_2 \left(\frac{A_2^3}{3} + \frac{A_5^3}{3} \right) - g z_1 \left(\frac{A_3^3}{3} + \frac{A_4^3}{3} \right)
 \end{aligned} \tag{3.1}$$

where as for Sect. 2.3, the $N \times N$ Hermitian matrices A_i with odd (resp. even) index correspond to black (resp. white) vertices, which can be empty (A_1, A_6), singly occupied (A_3, A_4) or doubly occupied (A_5, A_2). It is easy to check that the inverse of the quadratic

form in V generates the expected non-vanishing propagators $\langle A_1 A_2 \rangle$, $\langle A_1 A_4 \rangle$, $\langle A_1 A_6 \rangle$, $\langle A_5 A_6 \rangle$, $\langle A_3 A_6 \rangle$, $\langle A_3 A_4 \rangle$ (see Fig.7). Remarkably enough, the matrix interaction in V is simply chain-like, allowing for a solution using bi-orthogonal polynomials.

As before, the symmetry $A_i \leftrightarrow A_{7-i}$ of V ($i = 1, 2, 3$) ensures that the left and right polynomials are identical, hence we define the monic orthogonal polynomials p_n with respect to the appropriate symmetric scalar product, namely

$$(p_n, p_m) \equiv \int \prod_{i=1}^6 dx_i e^{-NV(x_1, x_2, x_3, x_4, x_5, x_6)} p_n(x_1) p_m(x_6) = h_n \delta_{n,m} \quad (3.2)$$

Introducing again the operators of multiplication by eigenvalues $Q_1, Q_2, Q_3, Q_4 = Q_3^\dagger, Q_5 = Q_2^\dagger, Q_6 = Q_1^\dagger$ and the operator P_1 of derivation with respect to eigenvalues of A_1 (all regarded as acting on $p_n(x_1)$), we find the master equations

$$\begin{aligned} \frac{P_1}{N} &= Q_2 - gQ_1^2 \\ 0 &= Q_1 - Q_3 - gz_2 Q_2^2 \\ 0 &= -Q_2 + Q_3^\dagger - gz_1 Q_3^2 \end{aligned} \quad (3.3)$$

which determine the h 's completely.

As a direct consequence of (3.3), the Q_i 's have a finite expansion in powers of the shift operator σ ($\sigma p_n = p_{n+1}$). The symmetry relation

$$V(\omega x_1, \omega^2 x_2, \omega x_3, \omega^2 x_4, \omega x_5, \omega^2 x_6) = V(x_1, x_2, x_3, x_4, x_5, x_6), \quad \omega = e^{2i\pi/3} \quad (3.4)$$

analogous to the case of hard objects on bicolored trivalent graphs, ensures that the relation (2.25) still holds for the orthogonal polynomials at hand. Then, using relations (3.3) and $\sigma^\dagger = \sigma^{-1}v$, where v is still defined as the diagonal operator with entries $v_n = h_n/h_{n-1}$, we find the expansions

$$\begin{aligned} Q_1 &= \sigma + \sum_{k=1}^{11} \sigma^{-3k+1} s^{(k)} \\ Q_2 &= g\sigma^2 + \sum_{k=1}^6 \sigma^{-3k+2} t^{(k)} \\ Q_3 &= -\sigma^4 g^3 z_2 + \sigma u^{(1)} + \sigma^{-2} u^{(2)} + \sigma^{-5} u^{(3)} + \sigma^{-8} u^{(4)} \end{aligned} \quad (3.5)$$

where the $s^{(k)}$, $t^{(k)}$ and $u^{(k)}$ are diagonal operators in the p_n basis. For simplicity we shall from now on go directly to the planar limit $n, N \rightarrow \infty$ as before with $x = n/N$ fixed, in

which the operators $s^{(k)}$, $t^{(k)}$ and $u^{(k)}$ become functions of x , while σ now plays the role of a dummy scalar expansion parameter. The last two lines of (3.3) allow clearly to express the $s^{(k)}$ and $t^{(k)}$ in terms of the $u^{(k)}$. Writing moreover the relation $Q_2 = Q_3^\dagger - gz_1Q_3^2$ at orders 8, 5, 2 in σ we may express $u^{(2)}$, $u^{(3)}$, $u^{(4)}$ as

$$\begin{aligned} u^{(2)} &= \frac{gv^2(1+z_1(u^{(1)})^2)}{1+2g^4z_1z_2v^2} \\ u^{(3)} &= -2g^4z_1z_2u^{(1)}v^5 \\ u^{(4)} &= g^7z_1z_2^2v^8 \end{aligned} \tag{3.6}$$

We finally get two equations determining $u^{(1)}$ and v implicitly in terms of x , by writing $Q_1 = Q_3 + gz_2Q_2^2$ at order 1 in σ and $P_1/N = Q_2 - gQ_1^2$ at order -1 in σ . Upon defining the rescaled quantities

$$\begin{aligned} \alpha &= \frac{z_1}{z_2} \\ V &= g^2z_2v \\ U &= z_2(u^{(1)})^2 \end{aligned} \tag{3.7}$$

we end up with the two equations

$$\begin{aligned} g^2z_2^2x &= \varphi(V, U) \equiv 4V^4(1-2\alpha^2V^4) - 2V^2 \frac{(1+\alpha U)^2}{(1+2\alpha V^2)^2} + V(1-20\alpha^2V^4)U \\ z_2 &= \psi(V, U) \equiv U \left(2V(1-4\alpha^2V^4) + \frac{(1-2\alpha V^2-4U\alpha^2V^2)}{(1+2\alpha V^2)} \right)^2 \end{aligned} \tag{3.8}$$

This system generalizes (2.29) in the sense that we must first solve the second equation for $U(V)$ as an implicit function of V (namely $z_2 = \psi(V, U(V))$) and plug it back into the first equation to get the relation $g^2z_2^2x = \varphi(V) \equiv \varphi(V, U(V))$, leading to the formula for the planar free energy through relation (2.15) (upon the substitution $g \rightarrow g^2z_2$ in the denominator of the Log). More precisely, the correct determination of U is dictated by the small x limit in which $v \sim x$, hence $V \sim g^2z_2x$ and $U \rightarrow z_2$.

Before we turn to the general study of the critical lines of the model, it is instructive to analyze the simple limiting cases discussed in Sect. 3.1, namely $u^{-1} \rightarrow 0$ ($z_1 \rightarrow 0$) for which we expect to recover the one-particle model of Sect. 2.3, and $(1/z_2) \rightarrow 0$ ($z_1, z_2 \rightarrow \infty$ with $u = z_2/z_1^2$ fixed) for which we expect a first order transition.

For $z_1 \rightarrow 0$, we simply take $\alpha = 0$ in (3.8) to write the second equation as $U = z_2/(1+2V)^2$ while the first equation gives $g^2z_2^2x = VU - 2V^2(1-2V)^2$. We therefore recover eqn. (2.29) with $z_2 \rightarrow z$.

More interestingly, in the other limit, we must let the parameters scale as $z_1 = \hat{z}_1/\epsilon$, $z_2 = \hat{z}_2/\epsilon^2$, $g = \hat{g}\epsilon$ with $\epsilon \rightarrow 0$. From (3.7) we deduce the other rescalings $\alpha = \hat{\alpha}\epsilon$, $V = \hat{V}$ and $U = \hat{U}/\epsilon^2$. In this limit, eqn. (3.8) becomes

$$\begin{aligned}\hat{g}^2 \hat{z}_1^2 x &= \frac{1}{2}(2\hat{U}\hat{V}\hat{\alpha}^2)(1 - (2\hat{U}\hat{V}\hat{\alpha}^2)) \\ \hat{z}_2 &= \hat{U}(2\hat{V} + 1 - 4\hat{U}\hat{V}^2\hat{\alpha}^2)^2\end{aligned}\tag{3.9}$$

The second line of (3.9) may be recast as

$$u^{-1} \frac{1}{2} \sqrt{\frac{\hat{U}}{\hat{z}_2}} \left(1 - \sqrt{\frac{\hat{U}}{\hat{z}_2}} \right) = \frac{1}{2}(2\hat{U}\hat{V}\hat{\alpha}^2)(1 - (2\hat{U}\hat{V}\hat{\alpha}^2))\tag{3.10}$$

with $u^{-1} = z_1^2/z_2 = \hat{z}_1^2/\hat{z}_2$ as before. This gives an alternative expression for $\hat{\varphi}(\hat{V}) \equiv \hat{g}^2 \hat{z}_1^2 x$. The maxima of $\hat{\varphi}(\hat{V})$ correspond clearly to either $2\hat{U}\hat{V}\hat{\alpha}^2 = 1/2$ or $\sqrt{\hat{U}/\hat{z}_2} = 1/2$ leading respectively to the critical values $\hat{g}_1^2 = 1/(8\hat{z}_1^2)$ or $\hat{g}_2^2 = u^{-1}/(8\hat{z}_1^2) = 1/(8\hat{z}_2)$. As before, the choice of the correct determination is best seen by considering the critical lines in the plane (\hat{V}, u^{-1}) . Using (3.10) with $2\hat{U}\hat{V}\hat{\alpha}^2 = 1/2$, we obtain the first curve

$$u^{-1} = \frac{\hat{z}_2 \hat{V} \hat{\alpha}^2}{2\sqrt{\hat{z}_2 \hat{V} \hat{\alpha}^2} - 1}\tag{3.11}$$

Using (3.10) with now $\sqrt{\hat{U}/\hat{z}_2} = 1/2$, we get the second curve

$$u^{-1} = \hat{z}_2 \hat{V} \hat{\alpha}^2 (2 - \hat{z}_2 \hat{V} \hat{\alpha}^2)\tag{3.12}$$

The curves (3.11) and (3.12) are plotted in Fig. 8. The solid portions correspond to the smallest values of \hat{V} for fixed u^{-1} which define the location of the relevant maxima of $\hat{\varphi}(\hat{V})$ attained by the change of variables $x \rightarrow \hat{V}$. The transition between the two curves takes place at $u = 1$ where \hat{g}^2 changes expression from \hat{g}_1^2 to \hat{g}_2^2 (see Fig. 9). This is clearly a first order transition as the slope of $\hat{g}^2(u)$ has a discontinuity at $u = 1$. Note also that $\hat{\varphi}''(\hat{V})$ is non-zero at the transition point, therefore we have $\gamma = -1/2$ as in the case of pure gravity.

Let us now turn to the general analysis of the complete phase diagram as obtained from eqn. (3.8). As before, we first look for critical lines characterized by $\varphi'(V) = 0 = \partial_V \varphi -$

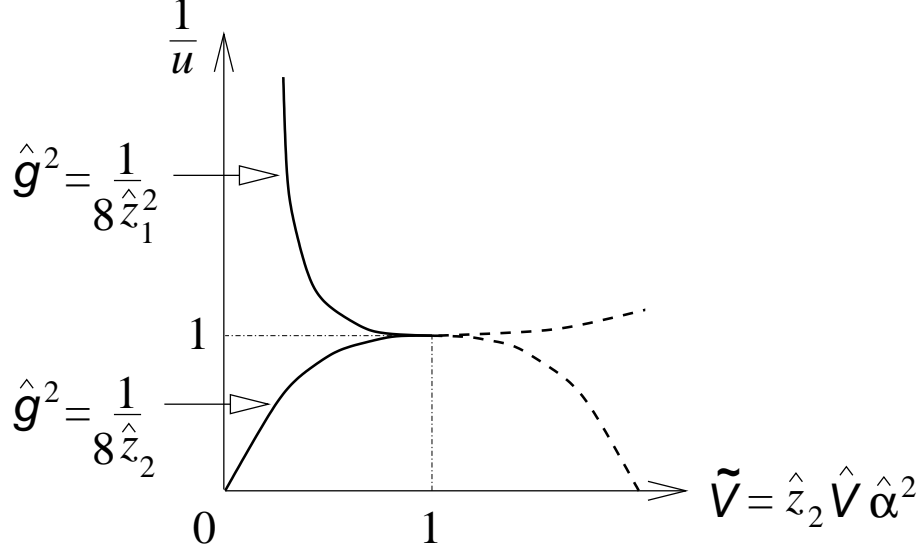


Fig. 8: Critical lines in the $(\tilde{V} \equiv \hat{z}_2 \hat{V} \hat{\alpha}^2, u^{-1})$ plane corresponding to $\hat{\varphi}'(\hat{V}) = 0$. The correct line corresponds to the lowest value of \tilde{V} and is represented by a solid line. The first order transition point $u^{-1} = 1$ is characterized by the contact between the two determinations of u^{-1} at which \hat{g}^2 jumps from $1/(8\hat{z}_2)$ to $1/(8\hat{z}_1^2)$.

$\partial_U \varphi(\partial_V \psi / \partial_U \psi)$. Using the explicit expressions for $\varphi(V, U)$ and $\psi(V, U)$, we immediately get two possible conditions:

$$\begin{aligned}
0 &= (1 - 2\alpha V^2)^2 (1 - 2V(1 + 2\alpha V^2)^2) + 4U\alpha^2 V^2 (1 + 6\alpha V^2) \\
0 &= 4V(1 + 2V(1 + 2\alpha V^2)^2)^2 \\
&\quad - U(1 - 8\alpha V(1 - V - 15\alpha V^3 - 52\alpha^2 V^5 - 50\alpha^3 V^7)) + 4U^2 \alpha^2 V
\end{aligned} \tag{3.13}$$

which leads to the three determinations: $U = U_0$ solution of the first line; $U = U_{\pm}$ conjugate solutions of the second line.

When substituted into $z_2 = \psi(V, U)$, this gives three branches in the plane (V, z_2) for fixed α . Let us now restrict ourselves to $z_1, z_2 > 0$, hence $\alpha > 0$. For small enough positive values of α the branches in the (V, z_2) plane take the generic form displayed in Fig. 10. As before, the correct solution corresponds to the smallest value of V for fixed z_2 , represented by solid lines in Fig. 10. We clearly identify two transitions at values $z_2^{(d)}$ and $z_2^{(c)}$. Comparing the qualitative behavior of the curves in the vicinity of the transition points with the behaviors obtained so far in the two above limiting cases, we can identify $z_2^{(d)}$ with a first order discontinuous transition point and $z_2^{(c)}$ with a continuous (critical Ising) transition point.

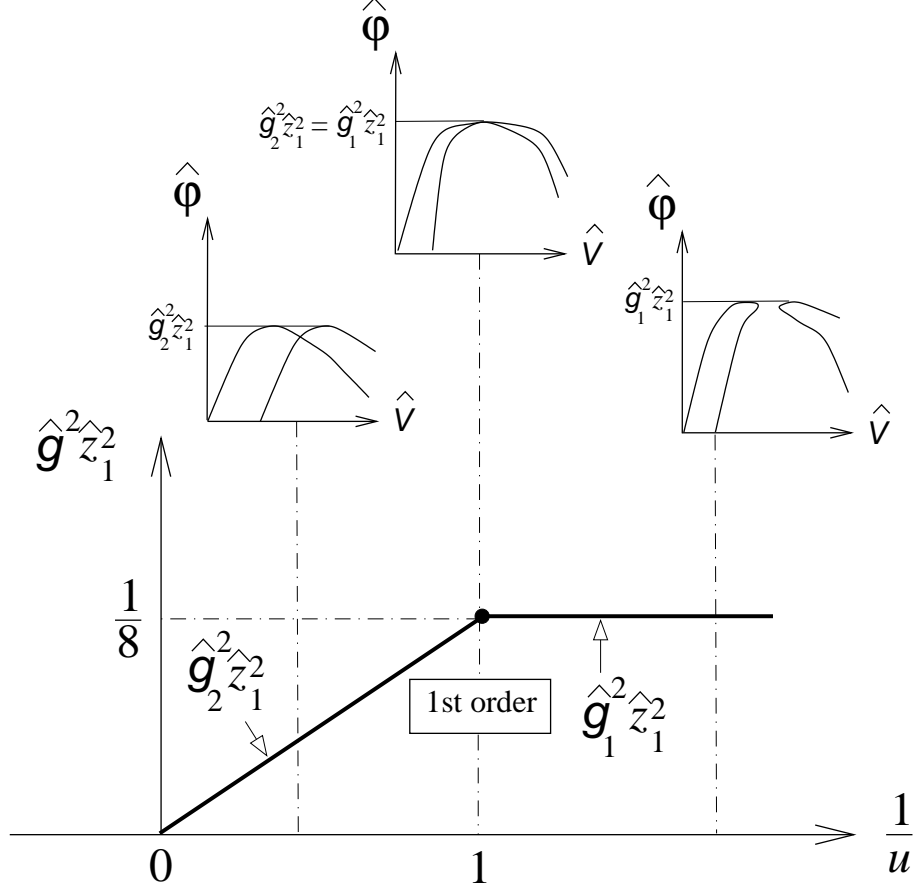


Fig. 9: Critical line in the $(u^{-1}, \hat{g}_1^2 \hat{z}_1^2)$ plane for the limiting case $z_1, z_2 \rightarrow \infty$, $u^{-1} = z_1^2/z_2$ fixed. The behaviors of $\hat{\phi}(\hat{V})$ below, at and above the transition are displayed in the small plots. The slope of $\hat{g}_1^2 \hat{z}_1^2$ is discontinuous at the first order transition point $u^{-1} = 1$.

The transition points correspond as illustrated in Fig. 10 to the coincidence of two branches. We can therefore obtain their location by expressing that $U_0 = U_+$ or $U_0 = U_-$, which is done explicitly by writing that the solution U_0 of the first line of (3.13) also satisfies the second line. We get the two possible conditions:

$$\begin{aligned}
0 &= 1 - V(1 - 2V^2\alpha - 20(V^2\alpha)^2 - 24(V^2\alpha)^3) \\
0 &= 1 - 20V^2\alpha + 100(V^2\alpha)^2 - 2V(1 - 16V^2\alpha - 104(V^2\alpha)^2 - 448(V^2\alpha)^3 + 400(V^2\alpha)^4)
\end{aligned}
\tag{3.14}$$

Introducing the variable $W = 2V^2\alpha$, we can express all the relevant quantities as rational

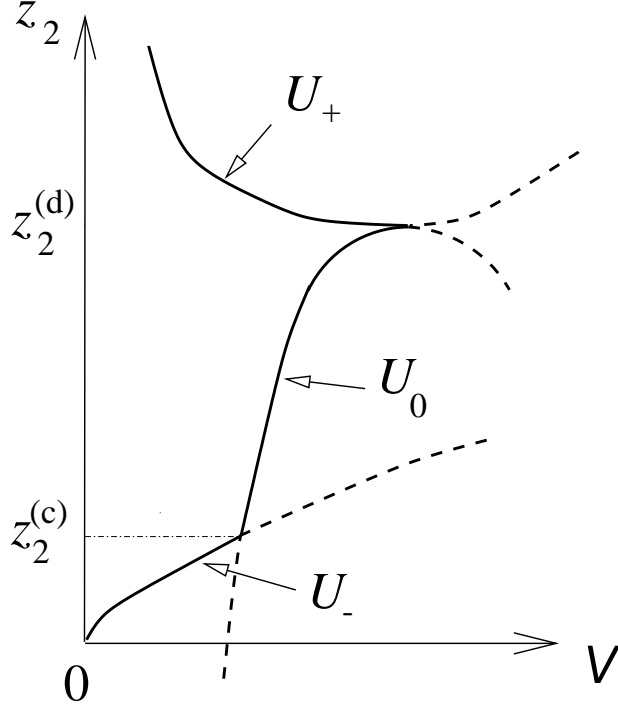


Fig. 10: Critical lines in the (V, z_2) plane for $z_2 > 0$ at some fixed (small enough) value of $\alpha = z_1/z_2$, as obtained by setting $\varphi'(V) = 0$. The solid lines correspond to the correct branches given by the smallest values of V . They correspond successively to the solutions U_- , U_0 and U_+ of eqn. (3.13). A continuous transition point occurs at the crossing point $z_2 = z_2^{(c)}$ of the two lowest branches, with a situation analogous to that found in Fig. 4 at the point $z = z_+$. A discontinuous transition point occurs at the contact point $z_2 = z_2^{(d)}$ between the two upper branches, with a situation analogous to that of Fig. 8 at the point $u^{-1} = 1$.

fractions of W . For the first line of (3.14) we end up with

$$\begin{aligned} \frac{1}{z_2} &= \frac{W^2(1+W)^6(1-3W)^5}{4(1-W)^6} \\ \frac{1}{u} &= \frac{(1-W)^6(1+W)^2}{1-3W} \end{aligned} \quad (3.15)$$

For the second line of (3.14) we get

$$\begin{aligned} \frac{1}{z_2} &= \frac{(1-8W-26W^2-56W^3+25W^4)^5}{32(1-W)^6(1-5W)^4(1-8W-25W^2)^2} \\ \frac{1}{u} &= \frac{128W^2(1-W)^6(1-8W-25W^2)^2}{(1-5W)^4(1-8W-26W^2-56W^3+25W^4)} \end{aligned} \quad (3.16)$$

It is easy to check that the points of the second curve (3.16) correspond to crossings of branches such as that happening at $z_2^{(c)}$ in Fig. 10. The situation around these points is

totally analogous to that described on Fig. 3 at the Ising transition point, with in particular $\varphi''(V) = 0$, henceforth $\gamma = -1/3$. We identify this curve with a line of continuous critical Ising transition points (CFT with $c = 1/2$ coupled to 2D quantum gravity).

The first curve (3.15) on the other hand corresponds to a contact of branches such as that encountered at $z_2^{(d)}$. The situation around this point is now similar to that found in Fig. 9 at the first order transition point. On this line we have $\varphi''(V) \neq 0$, hence $\gamma = -1/2$ as in the case of pure gravity (CFT with $c = 0$ coupled to 2D quantum gravity). However, the critical parameter g_c^2 has a discontinuity in its slope across this line, hence so does the free energy. We thus identify this curve with a line of first order transition points.

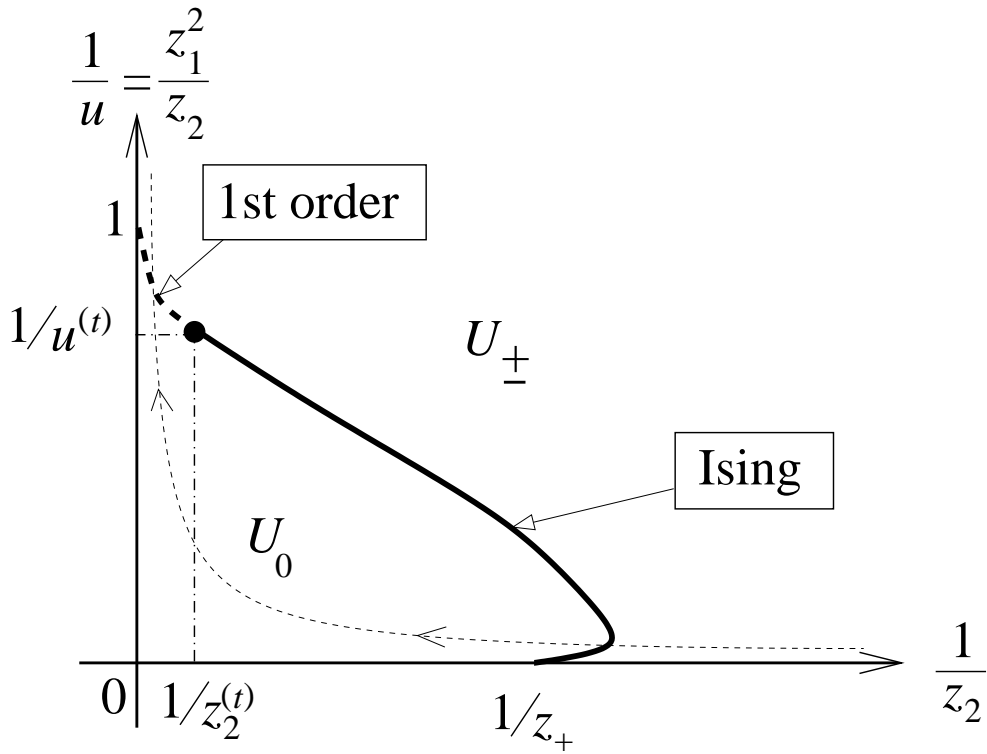


Fig. 11: The phase diagram of the two-particle exclusion model on random vertex bicolored planar lattices in the $(1/z_2, u^{-1})$ plane for $z_2 > 0$, as obtained from the exact solution of the six-matrix model (3.1). This phase diagram agrees with that of Fig. 6 with an Ising-like critical (solid) line meeting a first order (dashed) one at a tricritical Ising point (t). We have indicated the relevant branches of U solving eqn. (3.13), namely U_0 in the ordered phase, and U_{\pm} in the fluid one. We have also indicated a typical constant $\alpha = z_1/z_2$ hyperbola along which we encounter successively the two continuous and discontinuous transitions of Fig. 10.

These results are summarized in Fig. 11 where the first order transition line is represented by a dashed line and the continuous one by a solid line. These two lines meet at a

tricritical point with

$$\begin{aligned}
W^{(t)} &= \frac{\sqrt{41} - 6}{5} \\
\frac{1}{z_2^{(t)}} &= \frac{15633086927 - 2441464587\sqrt{41}}{80000000} = 0.00107319\dots \\
\frac{1}{u^{(t)}} &= \frac{32(-564779 + 87849\sqrt{41})}{78125} = 0.930177\dots
\end{aligned} \tag{3.17}$$

Note that Fig. 10 corresponds to a typical small enough constant α section (hyperbola in the $(1/z_2, u^{-1})$ plane) such as that represented in dotted line on Fig. 11 which crosses the two transition lines successively. The ordered phase lies below the transition lines and is described by the solution U_0 of the first line of (3.13) while the disordered phase lying above the transition curves corresponds to U_{\pm} solutions of the second line of (3.13).

The above phase diagram gives an *explicit* realization of that described qualitatively in Sect. 3.1. To complete our study, let us now show that the tricritical point (3.17) displays the expected behavior for a tricritical Ising transition point (CFT with $c(4, 5) = 7/10$) coupled to gravity. A first evidence comes from the fact that the string susceptibility exponent at this point is $\gamma = -1/4$ as $\varphi' = \varphi'' = \varphi''' = 0$ at this point while $\varphi^{(4)} \neq 0$. Note that the vanishing of φ'' holds generically for all points of the critical Ising line (3.16), as one readily checks by direct calculation. The vanishing of φ''' holds only at the tricritical point, as may be checked by a direct calculation too. The tricritical Ising CFT is the only unitary CFT with $\gamma = -1/4$ when coupled to gravity⁶. A second check can be performed by computing the thermal exponent α . More precisely, one can define two thermal exponents pertaining to two thermal operators with conformal dimensions $h_{33} = 1/10$ and $h_{32} = 3/5$, and the corresponding dressed dimensions when coupled to gravity $\Delta_{33} = 1/4$ and $\Delta_{32} = 3/4$. As explained in Appendix A, the most relevant one (Φ_{33}) governs the generic approach to the critical point through $f \sim (z_2 - z_2^{(t)})^{2-\alpha}$ with $\alpha = (1 - 2\Delta_{33})/(1 - \Delta_{33}) = 2/3$, while the other operator (Φ_{32}) governs the fine-tuned approach along a line tangent to the critical curves (3.15) and (3.16), with a behavior $f \sim (z_2 - z_2^{(t)})^{2-\alpha'}$ with $\alpha' = (1 - 2\Delta_{32})/(1 - \Delta_{32}) = -2$. To obtain the value of the first exponent in our model, a simple procedure consists in first fixing the ratio z_1/z_2 , expanding U for both lines of (3.13) in terms of $V - V^{(t)}$ and substituting the result into (3.8). We

⁶ $\gamma = -2/(p + q - 1)$ for a central charge $c(p, q)$ hence $p + q = 9$ and $q - p = 1$ by unitarity yield $p = 4, q = 5$.

finally get $g_c^2 - (g^{(t)})^2 = a(V - V^{(t)})^3 + b(V - V^{(t)})^4 + \dots$ and $z_2 - z_2^{(t)} = a'(V - V^{(t)})^3 + b'(V - V^{(t)})^4 + \dots$ which upon inversion leads to $g_c^2 - (g^{(t)})^2 = a''(z_2 - z_2^{(t)}) + b''(z_2 - z_2^{(t)})^{4/3}$ with values of a'' and $b'' \neq 0$ independent of the determination of U , hence $2 - \alpha = 4/3$ as expected. To get the second exponent, we may approach the tricritical point by traveling along the transition lines (3.15) and (3.16). For the first transition line we have

$$g_c^2 = \frac{W^2(1+W)^4(1-3W)^6(1-2W+3W^2+20W^3+3W^4-50W^5-35W^6)}{32(1-W)^{12}} \quad (3.18)$$

For the second transition line we have

$$g_c^2 = \frac{15(2-12W-41W^2+54W^3-19W^4)(1-8W-26W^2-56W^3+25W^4)^6}{8192(1-W)^{12}(1-5W)^2(1-8W-25W^2)^4} \quad (3.19)$$

Using the corresponding parametric values of z_2 (3.15) and (3.16) respectively, we easily check that the first three derivatives of g_c^2 with respect to z_2 match at the critical point $W = W^{(t)}$, while the fourth one is different. This discontinuity corresponds to $2 - \alpha' = 4$, hence $\alpha' = -2$.

For completeness let us finally discuss the case $z_1 > 0$ and $z_2 < 0$ ($u^{-1} < 0$). Looking again for the critical lines with $\varphi' = 0$, the relevant branch for U yielding the physical determination of φ is given by the second line of (3.13) i.e. $U = U_-$, say. Once substituted back into the second line of (3.8), this gives a critical line in the (V, z_2) plane, such as that plotted in Fig. 12 (a) (for $\alpha = z_1/z_2$ small enough). We recover the Lee-Yang singularity point at some $z_2^-(u)$, characterized by $\varphi''(V) = 0$ ($\gamma = -1/3$) due to the merging of the maximum of φ with its further minimum. Eliminating U , we finally obtain the following parametric curve

$$\begin{aligned} \frac{1}{z_2} &= -\frac{(5+100W+326W^2+820W^3-2275W^4)^5}{512(1-5W)^6(1+35W)^4(1+20W+35W^2)^2} \\ \frac{1}{u} &= -\frac{2048W^2(1-5W)^6(1+20W+35W^2)^2}{(1+35W)^4(5+100W+326W^2+820W^3-2275W^4)} \end{aligned} \quad (3.20)$$

with the parameter $W = -\alpha V^2 \geq 0$. In Fig. 12 (a), we note the existence of a further maximum of φ never attained by the change of variables $x \rightarrow V$ except when these three extrema merge simultaneously (see Fig. 12 (b)). This point corresponds to a higher order

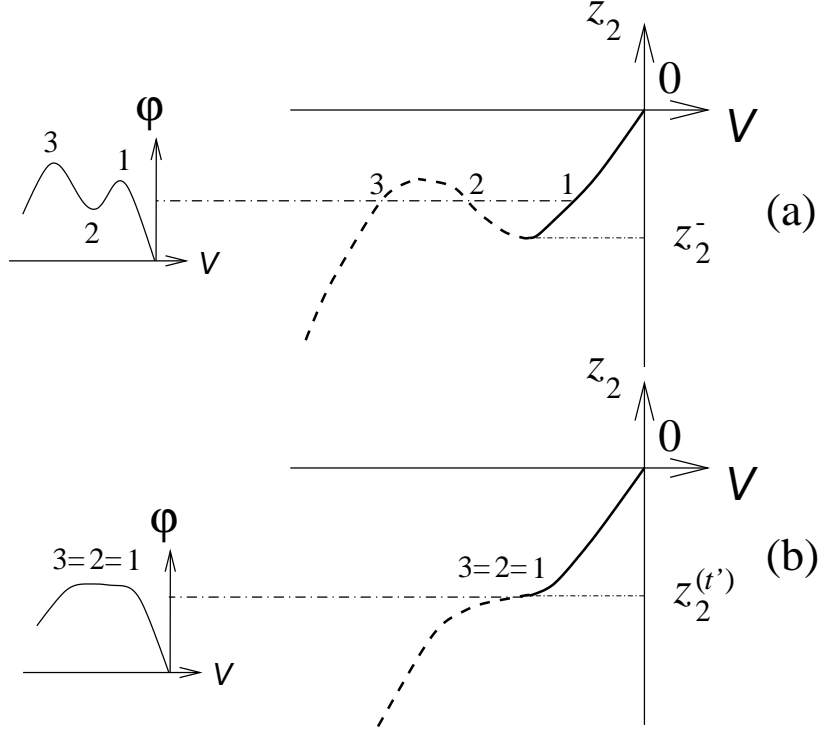


Fig. 12: Critical line in the (V, z_2) plane for $z_2 < 0$ as obtained by setting $\varphi'(V) = 0$ for fixed (small enough in modulus) $\alpha = z_1/z_2$. As usual, the correct portion of the curve corresponds to the lowest value of $|V|$ and is represented by a solid line. The Lee-Yang critical point z_2^- is characterized by $dz_2/dV = 0$ and corresponds to the merging and annihilation of the two extrema 1 and 2 in (a) with $\varphi''(V) = 0$. By increasing $|\alpha|$, we reach the situation (b) where a third extremum 3 merges with them. This defines the tricritical point $z_2^{(t')}$ satisfying in addition $\varphi'''(V) = 0$.

multicritical point with $\varphi''' = 0$, hence with a string susceptibility exponent $\gamma = -1/4$. This tricritical point corresponds to the values

$$\begin{aligned}
W^{(t')} &= \frac{8\sqrt{14} - 21}{455} \\
\frac{1}{z_2^{(t')}} &= -\frac{172647361044\sqrt{14} + 645414154777}{317007031250} = -4.07373\dots \\
\frac{1}{u^{(t')}} &= -\frac{524288(2401452\sqrt{14} - 8699159)}{10274243531825} = -0.0146072\dots
\end{aligned} \tag{3.21}$$

We thus conclude that the line of Lee-Yang critical points $z_2^-(u)$ ends at this higher critical point $z_2^{(t')}$. We identify this point with the only non-unitary CFT with $\gamma = -2/(p+q-1) = -1/4$, i.e. $c(2, 7) = -68/7$, coupled to 2D quantum gravity. A confirmation of this fact may be obtained by computing the thermal exponents of the theory α and α' characterizing

the singularity of the free energy (or equivalently of g_c^2) as z_2 approaches the tricritical value $z_2^{(t')}$. Like in the unitary case, the exponent α governs the generic approach to this point in the $(1/z_2, u^{-1})$ plane, while α' governs the fine-tuned approach along the line of Lee-Yang singular points. As shown in Appendix A, the predicted values are $\alpha = 2/3$ and $\alpha' = 1/2$. As before, we obtain the first exponent in our model by expanding g^2 and z_2 along a curve with, say, $z_1/z_2 = \text{const}$. We find generically $g_c^2 - (g^{(t')})^2 = a(V - V^{(t')})^3 + b(V - V^{(t')})^4 + \dots$ and $z_2 - z_2^{(t')} = a'(V - V^{(t')})^3 + b'(V - V^{(t')})^4 + \dots$ which upon inversion leads to $g_c^2 - (g^{(t')})^2 = a''(z_2 - z_2^{(t')}) + b''(z_2 - z_2^{(t')})^{4/3}$ with $b'' \neq 0$, which gives $2 - \alpha = 4/3$. To compute the second exponent, we use the parametric equations (3.20) and the corresponding value of g_c^2

$$g_c^2 = \frac{15(5 + 100W + 326W^2 + 820W^3 - 2275W^4)^6(2 - 60W + 151W^2 + 630W^3 - 2275W^4)}{2097152(1 - 5W)^{12}(1 + 35W)^2(1 + 20W + 35W^2)^4} \quad (3.22)$$

and expand g_c^2 and z_2 around the tricritical point $W^{(t')}$, with $g_c^2 - (g^{(t')})^2 = a(W - W^{(t')})^2 + b(W - W^{(t')})^3 + \dots$ and $z_2 - z_2^{(t')} = a'(W - W^{(t')})^2 + b'(W - W^{(t')})^3 + \dots$ which upon inversion leads to $g_c^2 - (g^{(t')})^2 = a''(z_2 - z_2^{(t')}) + b''(z_2 - z_2^{(t')})^{3/2}$ with $b'' \neq 0$, which gives $2 - \alpha' = 3/2$.

As discussed at the end of Sect. 2.2, the Lee-Yang critical line separates a small $|z_2|$ region where g_c is real from a large $|z_2|$ region where it becomes complex and generates an oscillatory behavior of the form (2.20) for the canonical partition function $Z_A(z_1, z_2)$ for planar graphs of fixed area A . This separation between oscillatory and non-oscillatory behaviors extends beyond the tricritical point (t') in the form of a first order transition line as depicted on Fig. 13. This line corresponds to a situation where the two complex conjugate values of g corresponding to the complex conjugate solutions to $\varphi' = 0$ cross in modulus the real value of g corresponding to the real solution to $\varphi' = 0$. The transition through this line is first order in the sense that the thermodynamic free energy has a discontinuous slope across the line. The line clearly originates at the tricritical point (t') where the three values of g are real and coincide. More interestingly, it is easy to see that it terminates at the point $(1/z_2, u^{-1}) = (0, -1)$. Indeed, along the axis $1/z_2 = 0$, we have to compare the real value $\hat{g}_1 = 1/\sqrt{8\hat{z}_1^2}$ and the two complex conjugate values $\hat{g}_2 = \pm i/\sqrt{8|\hat{z}_2|}$. For $u^{-1} > -1$, we have an oscillatory behavior of the partition function $\hat{Z}_A(\hat{z}_1, \hat{z}_2) = \lim \epsilon^A Z_A(z_1, z_2) \sim (-8\hat{z}_2)^{A/2}$, while for $u^{-1} < -1$ we simply have a non-oscillatory behavior $\hat{Z}_A(\hat{z}_1, \hat{z}_2) \sim (2\sqrt{2}\hat{z}_1)^A$.

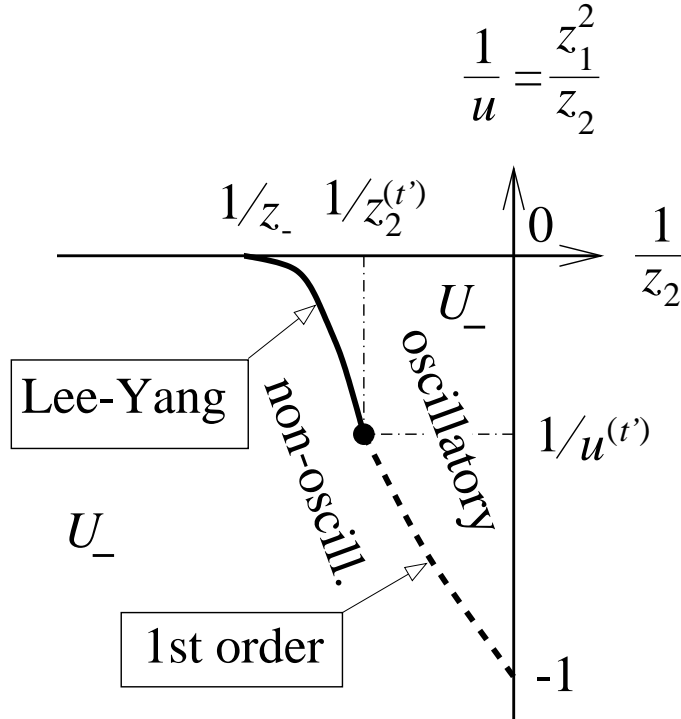


Fig. 13: The phase diagram of the two-particle exclusion model on random vertex bicolored planar lattices in the $(1/z_2, u^{-1})$ plane for $z_2 < 0$, as obtained from the exact solution of the six-matrix model (3.1). A (solid) line of Lee-Yang type critical points terminates at a tricritical point (t') where it meets another first order (dashed) transition line. These two lines form the border of the region of the phase diagram where an oscillatory behavior is observed in the canonical partition function $Z_A(z_1, z_2)$.

4. Conclusion and Discussion

In this paper, we have shown how to reach critical and multicritical points in the context of nearest neighbor exclusion models. We have displayed a number of exact solutions for various models defined on random planar lattices. The crucial outcome of this analysis is the importance of the colorability condition of the underlying lattice. Indeed, we have shown that critical points based on a \mathbb{Z}_2 symmetry such as the critical Ising and tricritical Ising models are reproduced for exclusion models under the condition that the lattice itself be vertex-bicolorable. In view of understanding the physics of the corresponding models on regular lattices, the outcome of the random lattice solutions is twofold: first it sorts out which features of the lattice itself take a relevant part in the models' critical behavior; secondly it allows for an exact solution in the planar limit that clearly identifies the critical universality classes for regular lattice models (such as the celebrated Hard Square model) which are still unsolved directly. More precisely, this study allows to infer that

the bipartite nature of the square and honeycomb lattices indeed translates into a critical Ising-like universality class for their crystallization transition point.

We have shown how to extend the definition of hard particle models to reach higher order critical points, by introducing a two-particle exclusion model in which each site may be empty, singly or doubly occupied with an exclusion constraint that a total of at most two particles may share the same edge. A straightforward generalization consists in having a k -particle exclusion model, where sites can be occupied by 0, 1, 2, ... up to k particles, with a weight z_i for an occupancy by i particles, and with the exclusion constraint that a total of at most k particles may share the same edge. When defined on a regular lattice, the exclusion constraint is easily turned into a non-overlapping constraint for appropriate tiles of various sizes. When defined on a random vertex-bicolorable lattice, these models are amenable to a $(2k + 2)$ matrix integral, with potential

$$V(A_1, A_2, \dots, A_{2k+2}) = \sum_{i=1}^{2k+1} (-1)^{i+1} A_i A_{i+1} - \frac{g}{3} \sum_{i=0}^k z_i (A_{2i+1}^3 + A_{2(k-i)+2}^3) \quad (4.1)$$

for trivalent graphs, with a weight g per vertex (and $z_0 = 1$). Remarkably enough, the exclusion rule translates into a chain-like quadratic interaction between the matrices, which makes the models exactly solvable by means of standard orthogonal polynomial techniques. With the model (4.1), we expect to be able to reach multicritical points governed by CFTs with central charges $c(p, q)$ with $p + q = 2k + 3$, by appropriately fine-tuning the z_i 's, in order to reach the highest possible critical string susceptibility exponent $\gamma = -1/(k + 2)$. We also expect the situation to be identical on vertex-bicolorable regular lattices.

One may also address the question of the behavior of the same particle exclusion models on lattices with other colorability properties. From the exact solution of the Hard Hexagon model on the triangular (hence vertex-tricolorable) lattice, it is natural to expect that the above exclusion models, when defined on vertex-tricolorable (fixed or random) lattices, give rise to critical and multicritical three-state Potts models. Unfortunately, the corresponding matrix models are no longer directly solvable by means of orthogonal polynomials.

More generally, the vertex- k -colorability of the lattice is likely to generate within the context of exclusion models critical points with \mathbb{Z}_k symmetry such as the k -state Potts model or the \mathbb{Z}_k model of Fateev and Zamolodchikov [20]. We know however that for large enough $k > 4$ we lose the continuous transition in the Potts case, while in the other

case the central charge $c = 2(k - 1)/(k + 2) > 1$ forbids any meaningful coupling to 2D quantum gravity.

Note finally that the above study provides an example of critical phenomena whose coupling to gravity is sensitive to the type of graphs summed over. While the precise connectivity (tri- or tetra-valency) of the lattices is unimportant, their Eulerian (bipartite) or Euclidean (arbitrary) character is relevant. This situation is reminiscent of that of fully-packed loop models [21,22].

Acknowledgments We thank T. Garel for a useful discussion on tricritical points and G. Akemann for a critical reading of the manuscript. J. B. is supported by the École normale supérieure.

Appendix A. String susceptibility and thermal exponents for minimal CFT coupled to 2D quantum gravity

The matrix models in general give a discretized version of matter systems coupled to 2D quantum gravity, in the form of discrete statistical models defined on random graphs accounting for the fluctuations of space-time. In the continuum approach to 2D quantum gravity, one may relate the properties of some critical matter system in fixed geometry (typically a CFT with central charge c in the plane) to that of the same matter system coupled to 2D quantum gravity. The precise connection involves the celebrated KPZ formula [23] expressing the string susceptibility exponent for a unitary CFT of central charge c coupled to 2D quantum gravity:

$$\gamma(c) = \frac{c - 1 - \sqrt{(1 - c)(25 - c)}}{12} \quad (\text{A.1})$$

as well as that the dimension Δ of the gravitational dressing ϕ of a primary operator of the CFT with dimension h :

$$\Delta(h, c) = \frac{\sqrt{1 - c + 24h} - \sqrt{1 - c}}{\sqrt{25 - c} - \sqrt{1 - c}} \quad (\text{A.2})$$

This dimension measures the singular behavior of the corresponding two-point correlator as $\langle \phi \phi \rangle \sim (\mu_c - \mu)^{2\Delta(h,c) - \gamma(c)}$, when the cosmological constant μ approaches its critical value μ_c . The above formulae simplify drastically when considering minimal CFT with central charge

$$c(p, q) = 1 - 6 \frac{(p - q)^2}{pq} \quad (\text{A.3})$$

with say $q \geq p + 1$ and $p \wedge q = 1$, and operator spectrum

$$h_{r,s} = \frac{(qr - ps)^2 - (p - q)^2}{4pq} \quad (\text{A.4})$$

with $qr - ps > 0$, $1 \leq r \leq p - 1$, $1 \leq s \leq q - 1$. Eqns. (A.1) and (A.2) reduce in this case to

$$\gamma(c(p, q)) = 1 - \frac{q}{p} \quad \Delta_{r,s} \equiv \Delta(h_{r,s}, c(p, q)) = \frac{(r - 1)q - (s - 1)p}{2p} \quad (\text{A.5})$$

For a unitary theory ($q = p + 1$), the most relevant operator of the theory is the identity with $h_{1,1} = 0$ and its gravitational dressing known as the ‘‘puncture operator’’ P has $\Delta_{1,1} = 0$ as well. This operator measures the area of the random surface, which allows to identify the deviation $\mu_c - \mu$ with $g_c - g$ in the corresponding matrix model, and to interpret $\gamma = -1/p$ as the exponent governing the singularity of the free energy. In the case of pure gravity ($p = 2, q = 3$), we have $\gamma = -1/2$, and the only operator is P . In the case of the critical Ising model ($p = 3, q = 4$) we have $\gamma = -1/3$ and three operators: the puncture P , the dressed energy operator $\Phi_{2,1}$ and the dressed spin operator $\Phi_{2,2}$, with respectively $\Delta_{1,1} = 0$, $\Delta_{2,1} = 2/3$ and $\Delta_{2,2} = 1/6$. The dressed energy is the thermal operator, with coupling $z_c - z \sim (\mu_c - \mu)^{1 - \Delta_{2,1}} = (g_c - g)^{1/3}$, hence upon inversion we get a singularity of the free energy of the form given by $g_c - g \sim (z_c - z)^{2 - \alpha}$, with $\alpha = -1$. In the case of the tricritical Ising model ($p = 4, q = 5$), we have $\gamma = -1/4$ and there are six operators, among which we distinguish the puncture P and the two thermal operators $\Phi_{3,3}$ and $\Phi_{3,2}$, with respectively $\Delta_{3,3} = 1/4$ and $\Delta_{3,2} = 3/4$. The generic thermal perturbation of the model is governed by the most relevant operator $\Phi_{3,3}$ with coupling $z_2 - z_2^{(t)} \sim (\mu_c - \mu)^{1 - \Delta_{3,3}} = (g_c - g)^{3/4}$, yielding the singularity of the free energy $g_c - g \sim (z_2 - z_2^{(t)})^{2 - \alpha}$ with $\alpha = 2/3$. By fine-tuning the parameters one may approach the tricritical point on a line along which the contribution of $\Phi_{3,3}$ is cancelled, and therefore the next most relevant thermal operator $\Phi_{3,2}$ takes over. This leads analogously to another thermal exponent α' with $2 - \alpha' = 1/(1 - \Delta_{3,2})$, hence $\alpha' = -2$.

For non-unitary theories with $q > p + 1$, the above formulae must be interpreted carefully to account for the fact that the identity is no longer the most relevant operator. Indeed, the scale of the deviation from criticality is set instead by the operator of smallest (negative) dimension $h_0 = (1 - (p - q)^2)/(4pq)$ (with $qr - ps = 1$) corresponding to the gravitationally dressed operator Φ_0 with dimension $\Delta_0 = (p - q + 1)/(2p)$. The latter operator has the coupling $(\mu_c - \mu)^{1 - \Delta_0}$ which allows to identify the deviation from criticality $(g_c - g)$ in the matrix model as $g_c - g = (\mu_c - \mu)^{1 - \Delta_0}$. Note that this general

relation also holds in the unitary case $q = p + 1$, where it reduces to $g_c - g = \mu_c - \mu$, as $h_0 = \Delta_0 = 0$. The most singular part of the free energy is due to the presence of Φ_0 and may be obtained by writing that $d^2 f/dg^2|_{\text{sing}} \sim \langle \Phi_0 \Phi_0 \rangle$. We can therefore write

$$\langle \Phi_0 \Phi_0 \rangle \sim (\mu_c - \mu)^{2\Delta_0 - \gamma(c(p,q))} \sim (g_c - g)^{-\gamma} \quad (\text{A.6})$$

from which we deduce the corrected string susceptibility exponent γ of the matrix model:

$$-\gamma = \frac{2\Delta_0 - \gamma(c(p,q))}{1 - \Delta_0} = \frac{2}{p + q - 1} \quad (\text{A.7})$$

To compute the thermal exponent we need to identify the next most relevant thermal operator say Φ_1 with dimension Δ_1 with coupling proportional to $(\mu_c - \mu)^{1 - \Delta_1} \sim (g_c - g)^{1/(2 - \alpha)}$, leading to $2 - \alpha = (1 - \Delta_0)/(1 - \Delta_1)$.

For the Lee-Yang edge singularity, we have $p = 2, q = 5$, and therefore $\Delta_0 = \Delta_{1,2} = -1/2$ and $\gamma = -1/3$. In this case, the deviation from the critical “temperature” $z_c - z$ is coupled to the next most relevant operator of the theory, which turns out to be the puncture operator $\Phi_1 = P$ with $\Delta_1 = 0$, leading to $\alpha = 1 + \Delta_0 = 1/2$. For the case $p = 2, q = 7$ of Sect. 3.2, we have $\Delta_0 = \Delta_{1,3} = -1$ and $\gamma = -1/4$. A generic deviation from criticality $z_2^{(t')} - z_2$ is coupled to the operator $\Phi_1 \equiv \Phi_{1,2}$ with $\Delta_1 = \Delta_{1,2} = -1/2$, hence yields a thermal exponent $\alpha = 2/3$. In a fine-tuned approach to the critical point, we may cancel the contribution of Φ_0 , in which case Φ_1 now plays the role of the most relevant operator, with $\Delta'_0 = \Delta_1$, while the thermal operator becomes P , with $\Delta'_1 = 0$. We deduce the fine-tuned thermal exponent $\alpha' = 1 + \Delta'_0 = 1 + \Delta_1 = 1/2$ identical to that of the Lee-Yang case.

Appendix B. Hard particles on a random tetravalent lattice: double scaling limit

In the following, we derive the double scaling limit of the model of hard particles on a random lattice (non-necessarily vertex-bicolorable). We show that the renormalized string susceptibility obeys the Lee-Yang differential equation. We first rewrite the eqns (2.11) and (2.12) in components, namely

$$\begin{aligned} \frac{n}{N} &= v_n - r_n - gz(s_n + s_{n+1} + s_{n+2} + r_n(r_{n-1} + r_n + r_{n+1})) \\ \tilde{r}_n &= v_n(1 + gz(r_{n-1} + r_n + r_{n+1})) \\ \tilde{s}_n &= gzv_nv_{n-1}v_{n-2} \end{aligned} \quad (\text{B.1})$$

and

$$\begin{aligned}
\frac{n}{N} &= v_n - g(\tilde{s}_n + \tilde{s}_{n+1} + \tilde{s}_{n+2} + \tilde{r}_n(\tilde{r}_{n-1} + \tilde{r}_n + \tilde{r}_{n+1})) \\
r_n &= gv_n(\tilde{r}_{n-1} + \tilde{r}_n + \tilde{r}_{n+1}) \\
s_n &= gv_nv_{n-1}v_{n-2}
\end{aligned} \tag{B.2}$$

Introducing the new coefficients

$$R_n = gr_n, \quad S_n = g^2s_n, \quad \tilde{R}_n = g\tilde{r}_n, \quad \tilde{S}_n = g^2\tilde{s}_n, \quad V_n = g\tilde{v}_n \tag{B.3}$$

we simply get

$$\begin{aligned}
\tilde{R}_n &= V_n(1 + z(R_{n-1} + R_n + R_{n+1})) \\
\tilde{S}_n &= zV_nV_{n-1}V_{n-2} \\
R_n &= V_n(\tilde{R}_{n-1} + \tilde{R}_n + \tilde{R}_{n+1}) \\
S_n &= V_nV_{n-1}V_{n-2} \\
g\frac{n}{N} &= V_n - \frac{R_n\tilde{R}_n}{V_n} - zV_n(V_{n-1}V_{n-2} + V_{n-1}V_{n+1} + V_{n+1}V_{n+2})
\end{aligned} \tag{B.4}$$

where both first lines of (B.1) and (B.2) turn out to be equivalent to the last line of (B.4). When N becomes large, all sequences tend to smooth functions of $x = n/N$, and setting $a = 1/N$, we now make the following scaling ansatz on $V_n \equiv V(x) = V(1 - a^2v(x))$, for some unknown function $v(x)$ for which we will derive a differential equation. We must first solve the first and third lines of (B.4) for $r(x)$ order by order in a , where $R_n \equiv R(x) = R(1 - a^2r(x))$, and where the values of V, R, z are taken along the critical line (2.18), namely with

$$z = \frac{12u(1+3u)^2}{(1-3u)^8}, \quad V = \frac{(1-3u)^4}{6(1+3u)}, \quad R = \frac{(1-3u)^7}{12(1+3u)^2} \tag{B.5}$$

with the result

$$\begin{aligned}
r(x) &= \frac{2v(x)}{1-3u} + a^2 \frac{1+9u}{3(1-3u)^2} (v''(x) - 3v(x)^2) - \frac{a^4}{36(1-3u)^3} ((1+54u+117u^2)v^{(4)}(x) \\
&\quad - 12(1+42u+81u^2)v(x)v''(x) - 288u(1+3u)v'(x)^2 + 432u(1+3u)v(x)^3) + O(a^6)
\end{aligned} \tag{B.6}$$

We now expand the last line of (B.4) up to order 6 in a , after setting u to its critical value $u_c = (2\sqrt{5} - 5)/15$, with the final result

$$\frac{g_c - gx}{g_c} = a^6(v(x)^3 - \frac{1}{2}v'(x)^2 - v(x)v''(x) + \frac{1}{10}v^{(4)}(x)) \tag{B.7}$$

Upon introducing the renormalized cosmological constant $y = (g_c - gx)/(a^{6/7}g_c)$ and appropriately rescaling $v(x) \rightarrow a^{-12/7}v(y)$, we finally get the standard differential equation for the renormalized string susceptibility $v(y)$

$$y = v(y)^3 - \frac{1}{2}v'(y)^2 - v(y)v''(y) + \frac{1}{10}v^{(4)}(y) \quad (\text{B.8})$$

which is easily identified with that of the Lee-Yang edge singularity coupled to 2D quantum gravity [9].

Appendix C. Hard particles on arbitrary random trivalent lattices

In the following we show that the trivalent lattice version of (2.1) leads to the same qualitative physics, namely a unique critical point in the universality class of the Lee-Yang edge singularity coupled to 2D quantum gravity.

We start with the trivalent version of the matrix model (2.1):

$$Z_N^{(3)}(g, z) = \int dA dB e^{-N \text{Tr} V(A, B)} \quad (\text{C.1})$$

$$V(A, B) = -\frac{1}{2}A^2 + AB - g\frac{B^3}{3} - gz\frac{A^3}{3}$$

where A, B are Hermitian with size $N \times N$, and the measure is normalized so that $Z_N^{(3)}(0, 0) = 1$. Comparing with (2.1), the bi-orthogonal polynomials are no longer even/odd as V is no longer even. We may still write the trivalent version of (2.7):

$$\begin{aligned} \frac{P_1}{N} &= Q_2^\dagger - Q_1 - gzQ_1^2 \\ \frac{P_2}{N} &= Q_1^\dagger - gQ_2^2 \end{aligned} \quad (\text{C.2})$$

and show that the Q 's have finite range, with

$$\begin{aligned} Q_1 &= \sigma + r + \sigma^{-1}s + \sigma^{-2}t \\ Q_2 &= \tau + \tilde{r} + \tau^{-1}\tilde{s} + \tau^{-2}\tilde{t} \end{aligned} \quad (\text{C.3})$$

where σ, τ denote the shift operators acting respectively on the left and right bi-orthogonal polynomials. In components, the equations (C.2) now read

$$\begin{aligned} \frac{n}{N} &= v_n - s_n - gz(t_n + t_{n+1} + s_n(r_{n-1} + r_n)) \\ \tilde{r}_n &= (r_n + gz(s_n + s_{n+1} + r_n^2)) \\ \tilde{s}_n &= v_n(1 + gz(r_n + r_{n-1})) \\ \tilde{t}_n &= gzv_nv_{n-1} \end{aligned} \quad (\text{C.4})$$

and

$$\begin{aligned}
\frac{n}{N} &= v_n - g(\tilde{t}_n + \tilde{t}_{n+1} + \tilde{s}_n(\tilde{r}_n + \tilde{r}_{n-1})) \\
r_n &= g(\tilde{s}_n + \tilde{s}_{n+1} + \tilde{r}_n^2) \\
s_n &= gv_n(\tilde{r}_{n-1} + \tilde{r}_n) \\
t_n &= gv_nv_{n-1}
\end{aligned} \tag{C.5}$$

For large n, N with $x = n/N$, we get algebraic equations for $V, R, S, T(x)$ respectively limits of $g^2zv_n, g^2zr_n, g^2zs_n, g^3zt_n$ and their tilded counterparts:

$$\begin{aligned}
g^2zx &= V - S - 2zT - 2RS \\
\tilde{R} &= R(1 + R) + 2zS \\
\tilde{S} &= V(1 + 2R) \\
\tilde{T} &= V^2 \\
R &= 2\tilde{S} + \tilde{R}^2/z \\
S &= 2V\tilde{R}/z \\
T &= V^2/z
\end{aligned} \tag{C.6}$$

easily solved in the form of an algebraic equation for R as a function of V

$$R \left(z - \frac{R(1 + R)^2}{(1 - 4V)^3} \right) = \frac{2zV}{1 - 4V} \tag{C.7}$$

and a master equation for the dependence on x :

$$g^2z^2x \equiv \varphi(V) = zV(1 - 2V) - 2 \frac{VR(1 + R)(1 + 2R)}{1 - 4V} \tag{C.8}$$

Writing that $\varphi' = \varphi'' = 0$, and eliminating z and V , we are left with a sixth order equation for the critical value of R , namely

$$13 + 266R + 1810R^2 + 5920R^3 + 10200R^4 + 8748R^5 + 2916R^6 = 0 \tag{C.9}$$

only one root of which leads to a positive value of g^2z^2 through (C.8) at $x = 1$. This leads to a unique critical point at

$$\begin{aligned}
R_c &= -0.090430\dots & V_c &= -0.036173\dots \\
z_c &= -0.16565\dots & g_c &= \sqrt{\varphi(V_c)}/|z_c| = 0.28105\dots
\end{aligned} \tag{C.10}$$

with the critical exponent $\gamma_{str} = -1/3$, and the critical point is in the (non-unitary) class of the Yang-Lee edge singularity as in the tetravalent case. It is easy to check that the scaling ansatz $V_n = V(1 - a^2v(x))$, $a = 1/N$, still leads, upon solving (C.4)(C.5) order by order in a , to the same differential equation (B.7) in which $g \rightarrow g^2z^2$.

Appendix D. Hard particles on trivalent bicolored graphs: double scaling limit

In the following, we complete the identification of both tricritical points (2.33) for the model (2.21) by deriving the corresponding differential equations for the renormalized version of the string susceptibility $V(x)$. To derive the double-scaling limit of the matrix model (2.21), let us first write in components the complete equations (2.28):

$$\begin{aligned}
s_n^{(0)} &= g \\
s_n^{(2)} &= -g^3 z v_n v_{n-1} v_{n-2} v_{n-3} \\
v_n &= s_n^{(1)} + g^2 z v_n (s_{n-1}^{(1)} + s_{n+1}^{(1)}) \\
r_n^{(1)} &= g v_{n-1} v_n + g^2 z (s_n^{(2)} + s_{n+2}^{(2)}) + g z s_n^{(1)} s_{n-1}^{(1)} \\
\frac{n}{N} &= s_n^{(1)} - g(r_n^{(1)} + r_{n+1}^{(1)})
\end{aligned} \tag{D.1}$$

Setting $V_n = g^2 z v_n$, $S_n = g^2 z s_n^{(1)}$, we finally get

$$\begin{aligned}
0 &= S_n - V_n(1 - S_{n-1} - S_{n+1}) \\
g^2 z^2 \frac{n}{N} &= z S_n(1 - S_{n-1} - S_{n+1}) - V_n(V_{n-1} + V_{n+1}) \\
&\quad + V_{n-1} V_n V_{n+1}(V_{n+2} + V_{n-2}) + V_n(V_{n-1} V_{n-2} V_{n-3} + V_{n+1} V_{n+2} V_{n+3})
\end{aligned} \tag{D.2}$$

We make the following scaling ansatz $V(x) = V(1 - a^2 v(x))$, $a = 1/N$ a small parameter. We first solve the equation $V_n(1 - S_{n-1} - S_{n+1}) = S_n$ order by order in a , with the result

$$\begin{aligned}
S(x) &= S(1 - a^2 s(x)) \\
s(x) &= \frac{v(x)}{1 + 2V} - a^2 \frac{V}{(1 + 2V)^2} v''(x) - a^2 \frac{2V}{(1 + 2V)^2} v(x)^2 - \frac{a^4 V(1 - 10V)}{12 (1 + 2V)^3} v^{(4)}(x) \\
&\quad + a^4 \frac{4V^2}{(1 + 2V)^3} v'(x)^2 - a^4 \frac{V(1 - 4V)}{(1 + 2V)^2} v(x) v''(x) + a^4 \frac{4V^2}{(1 + 2V)^3} v(x)^3 + O(a^6)
\end{aligned} \tag{D.3}$$

which we then substitute into the second line of (D.2) and Taylor-expand in a . Apart from the term of order zero, $\varphi(V) = g^2 t^2$, the lowest order terms are in a^6 . We then simply get at leading order

$$\begin{aligned}
\frac{g_i^2 t_i^2 - g^2 t^2 x}{g_i^2 t_i^2} &= a^6 (A_i v(x)^3 + B_i v(x) v''(x) + C_i v'(x)^2 + D_i v^{(4)}(x)) + O(a^8) \\
A_+ &= \frac{8}{15}, & A_- &= \frac{4}{3} \\
B_+ &= -\frac{6}{5}, & B_- &= -2 \\
C_+ &= -\frac{3}{5}, & C_- &= -1 \\
D_+ &= \frac{1}{5}, & D_- &= \frac{3}{10}
\end{aligned} \tag{D.4}$$

where the index $i = \pm$ refers to the critical point z_{\pm} . Upon setting $y = (g_i^2 t_i^2 - g^2 t^2 x)/(g_i^2 t_i^2 a^{6/7})$ and rescaling respectively $v(x) \rightarrow 9v(y)/(4a^{12/7})$ and $v(x) \rightarrow 3v(y)/(2a^{12/7})$, the differential equations take the standard form

$$\begin{aligned} (1) \quad & v^3 - vv'' - \frac{1}{2}(v')^2 + \frac{2}{27}v^{(4)} = y \\ (2) \quad & v^3 - vv'' - \frac{1}{2}(v')^2 + \frac{1}{10}v^{(4)} = y \end{aligned} \tag{D.5}$$

which we immediately identify with the differential equations governing the double scaling limit of respectively the Ising model and the Lee-Yang edge singularity [9].

Appendix E. Hard particles on tetravalent bicolored random graphs

The study is quite analogous to that of Sect. 2.3. The matrix integral takes the same form as (2.21), but with the potential

$$V(A_1, A_2, A_3, A_4) = A_1 A_2 - A_2 A_3 + A_3 A_4 - \frac{g}{4}(A_1^4 + A_4^4) - \frac{gz}{4}(A_2^4 + A_3^4) \tag{E.1}$$

We still have the symmetry $A_i \leftrightarrow A_{5-i}$ for $i = 1, 2$, hence introducing again a family of monic orthogonal polynomials p_n , and keeping notations as in (2.23), we get the two equations

$$\begin{aligned} \frac{P_1}{N} &= Q_2 - gQ_1^3 \\ 0 &= Q_1 - Q_2^\dagger - gzQ_2^3 \end{aligned} \tag{E.2}$$

The potential now satisfies the following additional symmetry property, replacing (2.24):

$$V(ix_1, -ix_2, ix_3, -ix_4) = V(x_1, x_2, x_3, x_4), \quad i^2 = -1 \tag{E.3}$$

The operators Q_1, Q_2 still have finite range, as a consequence of (E.2), and read, thanks to the symmetry (E.3):

$$\begin{aligned} Q_1 &= \sigma + \sum_{j=1}^7 \sigma^{1-4j} r^{(j)} \\ Q_2 &= g\sigma^3 + \sigma^{-1} s^{(1)} + \sigma^{-5} s^{(2)} + \sigma^{-9} s^{(3)} \end{aligned} \tag{E.4}$$

with the usual shift operator σ , with $\sigma^\dagger = \sigma^{-1}v$, where $v_n = h_n/h_{n-1}$ as usual, $h_n = (p_n, p_n)$ the square norm of p_n . The adjoint of Q_2 reads

$$Q_2^\dagger = g(\sigma^{-1}v)^3 + s^{(1)}v^{-1}\sigma + s^{(2)}(v^{-1}\sigma)^5 + s^{(3)}(v^{-1}\sigma)^9 \tag{E.5}$$

and the equations (E.2) boil down to

$$\begin{aligned}
s^{(3)} &= -g^4 z \sigma^9 (\sigma^{-1} v)^9 \\
s^{(2)} &= -g^3 z (\sigma^5 s^{(1)} + \sigma^2 s^{(1)} \sigma^3 + \sigma^{-1} s^{(1)} \sigma^6) (\sigma^{-1} v)^5 \\
s^{(1)} &= v - g z (\sigma s^{(2)} \sigma^{-1} + \sigma^{-2} s^{(2)} \sigma^2 + \sigma^{-5} s^{(2)} \sigma^5) \\
&\quad - g^2 z (\sigma^2 (s^{(1)} \sigma^{-1})^2 + \sigma^{-1} s^{(1)} \sigma^2 s^{(1)} \sigma^{-1} + \sigma^{-2} (s^{(1)} \sigma)^2) \\
r^{(1)} &= g \sigma^3 (\sigma^{-1} v)^3 + g z (s^{(3)} + \sigma^{-3} s^{(3)} \sigma^3 + \sigma^{-6} s^{(3)} \sigma^6) \\
&\quad + g^2 z (\sigma s^{(2)} \sigma^{-1} s^{(1)} + \sigma^5 \sigma^{(1)} \sigma^{-5} s^{(2)} + \sigma^{-2} s^{(2)} \sigma^2 s^{(1)} + \sigma^2 s^{(1)} \sigma^{-2} s^{(2)} \\
&\quad + \sigma^{-3} s^{(1)} \sigma s^{(2)} \sigma^2 + \sigma^2 s^{(1)} \sigma^{-5} s^{(2)} \sigma^3) + g z \sigma^3 (s^{(1)} \sigma^{-1})^3 \\
\frac{\nu}{N} &= s^{(1)} - g (r^{(1)} + \sigma^{-1} r^{(1)} \sigma + \sigma^{-2} r^{(1)} \sigma^2)
\end{aligned} \tag{E.6}$$

or equivalently in components:

$$\begin{aligned}
s_n^{(3)} &= -g^4 z v_n v_{n-1} \dots v_{n-8} \\
s_n^{(2)} &= -g^3 z v_n v_{n-1} \dots v_{n-4} (s_{n-5}^{(1)} + s_{n-2}^{(1)} + s_{n+1}^{(1)}) \\
s_n^{(1)} &= v_n - g z (g^2 (s_{n-1}^{(2)} + s_{n+2}^{(2)} + s_{n+5}^{(2)}) + g (s_{n-1}^{(1)} s_{n-2}^{(1)} + s_{n-1}^{(1)} s_{n+1}^{(1)} + s_{n+1}^{(1)} s_{n+2}^{(1)})) \\
r_n^{(1)} &= g v_n v_{n-1} v_{n-2} + g z (g^2 (s_n^{(3)} + s_{n+3}^{(3)} + s_{n+6}^{(3)}) + g (s_n^{(1)} s_{n-1}^{(2)} + s_n^{(2)} s_{n-5}^{(1)} + s_n^{(1)} s_{n+2}^{(2)} \\
&\quad + s_n^{(2)} s_{n-2}^{(1)} + s_{n+3}^{(1)} s_{n+2}^{(2)} + s_{n+3}^{(2)} s_{n-2}^{(1)}) + s_n^{(1)} s_{n-1}^{(1)} s_{n-2}^{(1)}) \\
\frac{n}{N} &= s_n^{(1)} - g (r_n^{(1)} + r_{n+1}^{(1)} + r_{n+2}^{(1)})
\end{aligned} \tag{E.7}$$

Upon the redefinitions

$$V_n = g v_n, \quad R_n = g^2 r_n^{(1)}, \quad S_n = g s_n^{(1)}, \quad T_n = g^2 s_n^{(2)}, \quad U_n = g^3 s_n^{(3)} \tag{E.8}$$

these equations finally reduce to

$$\begin{aligned}
U_n &= -z V_n V_{n-1} \dots V_{n-8} \\
T_n &= -z V_n V_{n-1} \dots V_{n-4} (S_{n-5} + S_{n-2} + S_{n+1}) \\
S_n &= V_n (1 - z (T_{n-1} + T_{n+2} + T_{n+5} + S_n S_{n-1} + S_{n-1} S_{n+1} + S_{n+1} S_{n+2})) \\
R_n &= V_n V_{n-1} V_{n-2} + z (U_n + U_{n+3} + U_{n+6} \\
&\quad + S_n T_{n-1} + T_n S_{n-5} + S_n T_{n+2} + T_n S_{n-2} + S_{n+3} T_{n+2} + T_{n+3} S_{n-2} + S_n S_{n-1} S_{n-2}) \\
g \frac{n}{N} &= S_n - (R_n + R_{n+1} + R_{n+2})
\end{aligned} \tag{E.9}$$

In the planar limit, each sequence tends to a function of $x = n/N$, $n, N \rightarrow \infty$, which we label by the same capital letter. Namely writing $U = -zV^9$, $T = -3zV^5S$, and also introducing $\Sigma = S/V$ we find

$$\begin{aligned} 1 &= \Sigma(1 - 9z^2V^6) + 3zV^2\Sigma^2 \\ gx \equiv \varphi(V) &= \Sigma V - 3(V^3 + zV^3\Sigma^3 - 18z^2V^7\Sigma^2 - 3z^2V^9) \\ &= -3V^3(1 - 3z^2V^6) + V\Sigma^2(1 + 45z^2V^6) \end{aligned} \quad (\text{E.10})$$

where we have used the first equation to simplify the second. The critical line is the solution of $\varphi'(V) = 0$. The first line of (E.10) allows to compute

$$\frac{d\Sigma}{dV} = \frac{6zV\Sigma(9zV^4 - \Sigma)}{1 + 6zV^2\Sigma - 9z^2V^6} \quad (\text{E.11})$$

Setting $W = zV^3$, we find

$$\varphi'(V) = -\frac{((1 - 5W)\Sigma - 3V(1 + W))((1 + 5W)\Sigma + 3V(1 - W))(2W\Sigma - V(1 - W^2))}{(2W\Sigma + V(1 - W^2))} \quad (\text{E.12})$$

hence we have three solutions

$$\begin{aligned} (1) \quad \Sigma &= \frac{3V(1 + W)}{1 - 5W} \\ (2) \quad \Sigma &= -\frac{3V(1 - W)}{1 + 5W} \\ (3) \quad \Sigma &= \frac{V(1 - W^2)}{2W} \end{aligned} \quad (\text{E.13})$$

The first line of (E.10) allows to express V in terms of W :

$$\begin{aligned} (1) \quad V &= \frac{1}{3(1 - 3W + 5W^2)} \left(\frac{1 - 5W}{1 + W} \right)^2 \\ (2) \quad V &= -\frac{1}{3(1 + 3W + 5W^2)} \left(\frac{1 + 5W}{1 - W} \right)^2 \\ (3) \quad V &= \frac{4W}{3(1 - W^2)^2} \end{aligned} \quad (\text{E.14})$$

We deduce the value of $z = \frac{W}{3V^3}$:

$$\begin{aligned} (1) \quad z &= \frac{9W(1 + W)^6(1 - 3W + 5W^2)^3}{(1 - 5W)^6} \\ (2) \quad z &= -\frac{9W(1 - W)^6(1 + 3W + 5W^2)^3}{(1 + 5W)^6} \\ (3) \quad z &= \frac{9(1 - W^2)^6}{64W^2} \end{aligned} \quad (\text{E.15})$$

and finally that of $g = \varphi(V)$:

$$\begin{aligned}
(1) \quad g &= \frac{2(1-5W)^4(3+24W-10W^2+40W^3+35W^4)}{27(1+W)^6(1-3W+5W^2)^3} \\
(2) \quad g &= \frac{2(1+5W)^4(3-24W+10W^2-40W^3+35W^4)}{27(1-W)^6(1+3W+5W^2)^3} \\
(3) \quad g &= \frac{16W(1+W^2)(1-10W+5W^2)}{27(1-W^2)^6}
\end{aligned} \tag{E.16}$$

The tricritical points are solution in addition of $\varphi''(V) = 0$. In the three above case, we get

$$\varphi''(V) = \begin{cases} \frac{18V(1-12W+5W^2)(-1-20W+35W^2)}{(1-5W)^2} & \text{in case (1)} \\ \frac{18V(1+12W+5W^2)(-1+20W+35W^2)}{(1+5W)^2} & \text{in case (2)} \\ -\frac{3V}{16W^2}(1+5W^2)(1-12W+5W^2)(1+12W+5W^2) & \text{in case (3)} \end{cases} \tag{E.17}$$

As in the trivalent case of Sect. 2.3, each of the lines (1) and (2) have two tricritical points, one of which is a cusp, the other coming from the intersection with the critical curve (3). Moreover the curve (1) is always reached before (2). The cusp solves $1+20W-35W^2=0$, while the intersection solves $1-12W+5W^2=0$. Again, one of the two branches of these equations is always reached before the other. We end up with a qualitative picture identical to that of Fig.3, with the cusp and intersection corresponding respectively to the values W_{\pm} :

$$W_- = \frac{10-3\sqrt{15}}{35}, \quad W_+ = \frac{6-\sqrt{31}}{5} \tag{E.18}$$

while the tricritical point corresponds to the values (z_{\pm}, g_{\pm}) given by the case (1) in (E.16) and (E.15), respectively with $W = W_{\pm}$ of (E.18), with the exact values

$$\begin{aligned}
z_- &= -\frac{15683(-83151+26080\sqrt{15})}{2573571875} = -.136568... \\
g_- &= \frac{2000(129105-24881\sqrt{15})}{235782657} = .277724... \\
z_+ &= \frac{6561(146327-21472\sqrt{31})}{9765625} = 17.989334... \\
g_+ &= \frac{80(14903-1067\sqrt{31})}{14348907} = .049967...
\end{aligned} \tag{E.19}$$

To get the double scaling limit, we set

$$V_n = V(1-a^2v(x)), \quad S_n = \Sigma V(1-a^2s(x)) \tag{E.20}$$

and first solve the third equation of (E.9) order by order in a , with the result

$$\begin{aligned}
s(x) &= \frac{1-5W}{1+W}v(x) + a^2 \frac{W(1-5W)(3-10W+5W^2)}{(1+W)^2(1+5W^2)}(3v^2(x) - 2v''(x)) \\
&\quad - a^4 \frac{W(1-5W)(3-155W+650W^2-1530W^3+1375W^4-175W^5)}{(1+W)^3(1+5W^2)}v(x)^3 \\
&\quad + a^4 \frac{W(1-5W)(3-205W+355W^2-85W^3)}{(1+W)^3(1+5W^2)}v'(x)^2 \\
&\quad + a^4 \frac{12W(1-5W)(1-29W+70W^2-190W^3+225W^4-25W^5)}{(1+W)^3(1+5W^2)^2}v(x)v''(x) \\
&\quad - a^4 \frac{W(1-5W)(9-445W+721W^2-121W^3)}{(1+W)^3(1+5W^2)}v^{(4)}(x) + O(a^6)
\end{aligned} \tag{E.21}$$

We then substitute this and (E.20) into the last line of (E.9), and Taylor-expand in a . The final result reads

$$\begin{aligned}
\frac{g_i - g_x}{g_i} &= a^6(A_i v(x)^3 + B_i v(x)v''(x) + C_i v'(x)^2 + D_i v^{(4)}(x)) + O(a^8) \\
A_- &= \frac{5}{2}D_- \quad A_+ = \frac{3}{2}D_+ \\
B_- &= -5D_- \quad B_+ = -\frac{9}{2}D_+ \\
C_- &= -\frac{5}{2}D_- \quad C_+ = -\frac{9}{4}D_+ \\
D_- &= \frac{27(5-3\sqrt{15})}{110} \quad D_+ = \frac{291-49\sqrt{31}}{5125}
\end{aligned} \tag{E.22}$$

which may be put back in the standard forms (D.5). We conclude that the situation for the hard particle model on vertex-bicolorable tetravalent random lattices is qualitatively the same as that for trivalent ones: we find two critical points at $z_- = -.136568\dots$ and $z_+ = 17.989334\dots$ respectively in the universality classes of the Lee-Yang and Ising critical models on random lattices. Note that this model is precisely the gravitational version of the classical Hard Square model, as, in the dual picture we are considering non-overlapping square tiles on random, face-bicolorable planar quadrangulations (dual to planar tetravalent vertex-bicolorable random lattices), hence a random version of the square lattice incorporating its vertex-bicolorability.

References

- [1] R. J. Baxter, *Hard Hexagons: Exact Solution*, J. Phys. **A 13** (1980) L61-L70; R. J. Baxter and S.K. Tsang, *Entropy of Hard Hexagons*, J. Phys. **A 13** (1980) 1023-1030; see also R. J. Baxter, *Exactly Solved Models in Statistical Mechanics*, Academic Press, London (1984).
- [2] J. Cardy, *Conformal Invariance and the Yang-Lee Edge Singularity in Two Dimensions*, Phys. Rev. Lett. **54**, No. 13 (1985) 1354-1356.
- [3] P. Di Francesco, H. Saleur and J.-B. Zuber, *Generalized Coulomb Gas Formalism for Two-dimensional Critical Models based on $SU(2)$ Coset Construction*, Nucl. Phys. **B300** [FS] (1988) 393-432.
- [4] H. Takasaki, T. Nishino and Y. Hieida, *Phase Diagram of a 2D Vertex Model*, J. Phys. Soc. Japan Vol. **70** (2001) 1429-1430, preprint cond-mat/0012490.
- [5] R. J. Baxter, *Planar Lattice Gases with Nearest-neighbour Exclusion*, Annals of Combin. No. **3** (1999) 191-203 preprint cond-mat/9811264.
- [6] R. J. Baxter, I. G. Enting and S.K. Tsang, *Hard Square Lattice Gas*, J. Stat. Phys. **22** (1980) 465-489.
- [7] D. Gaunt and M. Fisher, *Hard-Sphere Lattice Gases. I. Plane-Square Lattice*, J. Chem. Phys. **43** (1965) 2840-2863.
- [8] L. Runnels, L. Combs and J. Salvant, *Exact Finite Methods of Lattice Statistics. II. Honeycomb-Lattice Gas of Hard Molecules*, J. Chem. Phys. **47** (1967) 4015-4020.
- [9] P. Di Francesco, P. Ginsparg and J. Zinn-Justin, *2D Gravity and Random Matrices*, Physics Reports **254** (1995) 1-131.
- [10] B. Eynard, *Random Matrices*, Saclay Lecture Notes (2000), http://www-spht.cea.fr/lectures_notes.shtml
- [11] D. Kurze and M. Fisher, *Yang-Lee Edge Singularities at High Temperatures*, Phys. Rev. **B20** (1979) 2785-2796.
- [12] P. Di Francesco and E. Guitter, *Critical and Multicritical Semi-Random $(1+d)$ -Dimensional Lattices and Hard Objects in d Dimensions*, preprint cond-mat/0104383 (2001), to appear in J. Phys. **A** (2002).
- [13] M. Staudacher, *The Yang-Lee Edge Singularity on a Dynamical Planar Random Surface*, Nucl. Phys. **B336** (1990) 349-362.
- [14] E. Brézin, C. Itzykson, G. Parisi and J.-B. Zuber, *Planar Diagrams*, Comm. Math. Phys. **59** (1978) 35-51.
- [15] L. Chekhov and C. Kristjansen, *Hermitian Matrix Model with Plaquette Interaction*, Nucl. Phys. **B479** (1996) 683-696.
- [16] W. Tutte, *A Census of Planar Maps*, Canad. Jour. of Math. **15** (1963) 249-271.
- [17] P. Di Francesco, B. Eynard and E. Guitter, *Coloring Random Triangulations*, Nucl. Phys. **B516** [FS] (1998) 543-587.

- [18] M. Blume, V. Emery and R. Griffiths, *Ising Model for the λ Transition and Phase Separation in He^3 - He^4 Mixtures*, Phys. Rev. **A4** (1971) 1071-1077.
- [19] I. Lawrie and S. Sarbach, *Theory of Tricritical Points*, in *Phase Transitions and Critical Phenomena*, vol. 9, C. Domb and J. Lebowitz eds., Academic Press, London (1984).
- [20] V.A. Fateev and A.B. Zamolodchikov, *Selfdual Solutions of the Star-triangle Relations in \mathbb{Z}_N Models*, Phys. Lett. **A92** (1982) 37-39; A.B. Zamolodchikov and V.A. Fateev, *Nonlocal (Parafermion) Currents in Two-dimensional Conformal Quantum Field Theory and Self-dual Critical Points in \mathbb{Z}_n -symmetric Statistical Systems*, Sov. Phys. J.E.T.P. **62** (1985) 215-225.
- [21] E. Guitter, C. Kristjansen and J.L. Nielsen *Hamiltonian Cycles on Random Eulerian Triangulations* Nucl. Phys **B546[FS]** (1999) 731-750.
- [22] P. Di Francesco, E. Guitter and C. Kristjansen *Fully Packed $O(n=1)$ Model on Random Eulerian Triangulations* Nucl. Phys **B549[FS]** (1999) 657-667.
- [23] V.G. Knizhnik, A.M. Polyakov and A.B. Zamolodchikov, *Fractal Structure of 2D Quantum Gravity*, Mod. Phys. Lett. **A3** (1988) 819-826; F. David, *Conformal Field Theories Coupled to 2D Gravity in the Conformal Gauge*, Mod. Phys. Lett. **A3** (1988) 1651-1656; J. Distler and H. Kawai, *Conformal Field Theory and 2D Quantum Gravity*, Nucl. Phys. **B321** (1989) 509-527.